

# Assessment of uranium nitride interatomic potentials

Mohamed AbdulHameed<sup>a</sup>, Benjamin Beeler<sup>a,b,\*</sup>, Conor O.T. Galvin<sup>c</sup>, Michael W.D. Cooper<sup>c</sup>

<sup>a</sup>*Department of Nuclear Engineering, North Carolina State University, Raleigh, NC 27695*

<sup>b</sup>*Idaho National Laboratory, Idaho Falls, ID 83415*

<sup>c</sup>*Los Alamos National Laboratory, Los Alamos, NM 87545*

---

## Abstract

Uranium mononitride (UN) is a promising nuclear fuel due to its high fissile density, high thermal conductivity, and suitability for reprocessing. In this study, two uranium nitride interatomic potentials are assessed: Tseplyaev and Starikov's angular-dependent potential and Kocevski *et al.*'s embedded atom model potential. Predictions of the thermophysical and elastic properties of UN, UN<sub>2</sub>, and  $\alpha$ - and  $\beta$ -U<sub>2</sub>N<sub>3</sub> computed using both potentials are assessed and compared to available experimental data. The Tseplyaev potential performs better with the energetic aspects of UN, e.g., specific heat capacity and point defect formation energies, whereas the Kocevski potential performs better with the structural aspects of UN, e.g., thermal expansion as well as with the elastic properties. The reasons why the Kocevski potential underestimates the UN specific heat are explained by examining the UN phonon properties modeled using both potentials. The Kocevski potential shows better identification of the mechanical stability ranges of UN, UN<sub>2</sub>, and  $\alpha$ - and  $\beta$ -U<sub>2</sub>N<sub>3</sub>, reasonably predicting the melting point of UN and predicting stable structures for UN<sub>2</sub> and  $\alpha$ - and  $\beta$ -U<sub>2</sub>N<sub>3</sub>. On the other hand, the Tseplyaev potential predicts a premature phase change of both UN and UN<sub>2</sub> and cannot stabilize  $\alpha$ - nor  $\beta$ -U<sub>2</sub>N<sub>3</sub>. However, the Kocevski potential cannot predict a stable  $\alpha$ -U phase and is thus not suitable for the calculation of formation energies for non-stoichiometric point defects.

*Keywords:* uranium nitride, thermophysical properties, molecular dynamics, phonons, point defects

---

## 1. Introduction

Since the 2011 Fukushima Daiichi accident in Japan, research efforts have been directed to develop advanced nuclear fuels that have improved performance in extreme conditions compared to UO<sub>2</sub> while maintaining thermodynamic and mechanical stability [1]. One such fuel candidate is uranium mononitride (UN), which has shown many positive characteristics including high fissile density, high thermal conductivity, good dissolution in nitric acid making it compatible with the PUREX process, good chemical compatibility with most potential cladding materials, and longer fuel residence time [2, 3, 4]. However, it has also

---

\*Corresponding author

Email address: bwbeeler@ncsu.edu (Benjamin Beeler)

9 suffered some drawbacks that historically hindered its industrial adoption, including com-  
10 plicated fabrication processes, high fuel cost owing to the need for N-15 enrichment, low  
11 resistance to oxidation by high-temperature steam, and high swelling rates [2, 3, 4].

12 UN has not been investigated as widely as oxide fuels, and many aspects of its behavior  
13 at high temperatures and under irradiation are not well understood [5]. To address its  
14 drawbacks and build a case for its practical use in light-water and advanced reactors, UN  
15 properties should be well-understood at the atomic and mesoscales. Multiscale multiphysics  
16 fuel performance models can provide a pathway for the descriptive and predictive evolution  
17 of nuclear fuels and are especially valuable in cases where experimental data is limited. These  
18 models, however, require many input parameters from lower-length scale simulation methods  
19 like density functional theory (DFT) and molecular dynamics (MD).

20 Many DFT studies have been conducted on UN to predict its electronic structure and  
21 magnetic ordering [6, 7, 8, 9, 10] as well as to understand the properties of its point de-  
22 fects [11, 12, 13, 14], impurities [15], and fission products [16, 17, 18, 19]. However, DFT is  
23 computationally demanding and has limitations in system size and simulation time. MD sim-  
24 ulations can overcome these limitations and offer more flexibility in predicting fuel behavior  
25 at finite temperatures. Still, the accuracy of MD results is highly dependent on the quality  
26 of the interatomic potentials employed. Therefore, a reliable UN interatomic potential is a  
27 necessity.

28 For UN, several interatomic potentials exist in the literature. Kurosaki *et al.* [20, 21] de-  
29 veloped a Busing-Ida type potential which they used to predict thermal expansion, constant-  
30 pressure specific heat capacity, and thermal conductivity. Calculated properties qualitatively  
31 agree with experimental results at low temperatures and exhibit an increasing underestima-  
32 tion with increasing temperature. Kurosaki *et al.* mention the values of potential parameters  
33 without units, which makes it hard to further assess its behavior. Chen *et al.* [22] used the  
34 Chen–Möbius lattice inversion method to derive three Morse-type pair potentials for the  
35 U-U, N-N, and U-N interactions. The potential was then used to predict thermal expansion  
36 and compressibility with a moderate qualitative agreement. However, Morse-type potentials  
37 cannot capture the nature of atomic bonding, especially in covalent solids such as UN [23].

38 Kuksin *et al.* [24] developed an angular-dependent potential (ADP) fitted to DFT calcu-  
39 lations. The potential was modified in a later paper by Tseplyaev and Starikov [25], and used  
40 to calculate point defect formation and migration energies and to predict the UN pressure-  
41 induced  $Fm\bar{3}m \rightarrow R\bar{3}m$  phase transition. However, the authors didn't consider the effect of  
42 stoichiometry on defect formation energies, and their methodology to calculate the U and  
43 N chemical potentials is not reported. They also show evidence of the potential's capability  
44 to predict some basic properties of  $UN_2$  and  $U_2N_3$ . Li and Murphy [26] have later used this  
45 potential to study self-diffusion in hypo-stoichiometric UN.

46 Kocevski *et al.* [27] developed an embedded-atom method (EAM) potential fitted to  
47 experimental thermal expansion and single crystal elastic constants, as well as formation  
48 energies of stoichiometric point defects from DFT calculations. The potential reproduced  
49 observed elastic properties and temperature-dependent heat capacity with reasonable agree-  
50 ment and was also used to study Xe diffusion in UN.

51 Tseplyaev and Starikov's ADP (hereafter referred to as the Tseplyaev potential) and Ko-  
52 cevski *et al.*'s EAM potential (hereafter referred to as the Kocevski potential) are promising  
53 candidate potentials by their construction that attempts to model the complex bonding en-

54 vironment of UN. The main goal of this work is to assess the performance of both potentials  
 55 and to identify their relevant artifacts and weaknesses by performing MD simulations that  
 56 calculate UN elastic properties, specific heat capacity, and phonon properties. We also cal-  
 57 culate point defect formation energies using a methodology that removes the arbitrariness in  
 58 chemical potential determination. Thermophysical and elastic properties of  $\text{UN}_2$  and  $\text{U}_2\text{N}_3$   
 59 phases are also computed, and their predicted stability is discussed.

## 60 2. Computational details

61 All MD calculations performed in this work utilize the Large-scale Atomic/Molecular  
 62 Massively Parallel Simulator (LAMMPS) software package [28] with a time step of 1 fs  
 63 and periodic boundary conditions applied in all directions. The Phonopy code [29] is used  
 64 to calculate phonon properties. To obtain the forces calculated by LAMMPS in a format  
 65 readable by Phonopy, PhonoLAMMPS, an auxiliary tool of the DynaPhoPy code [30], is  
 66 used. Detailed computational methodologies of all properties are presented in the respective  
 67 sections.

### 68 2.1. Structural properties

69 The U-N solid system has three distinct compounds: UN, uranium dinitride ( $\text{UN}_2$ ), and  
 70 uranium sesquinitride ( $\text{U}_2\text{N}_3$ ) [31]. UN has a NaCl crystal structure with a lattice parameter  
 71  $a = 4.89 \text{ \AA}$  at room temperature [32] and a melting temperature  $T_m = 3035 \text{ K}$  at a nitrogen  
 72 vapor pressure of 1 atm [33].  $\text{UN}_2$  has a fluorite crystal structure with an experimental  
 73 lattice parameter  $a = 5.21 \text{ \AA}$  [34].  $\text{U}_2\text{N}_3$  has a bixbyite crystal structure at low temperatures  
 74 ( $\alpha\text{-U}_2\text{N}_3$ ) and a hexagonal crystal structure at high temperatures ( $\beta\text{-U}_2\text{N}_3$ ) [4].  $\alpha\text{-U}_2\text{N}_3$  has  
 75 a space group:  $Ia\bar{3}$ , and a lattice parameter of  $10.7 \text{ \AA}$ , whereas  $\beta\text{-U}_2\text{N}_3$  has a space group:  
 76  $P\bar{3}m1$ , Pearson symbol:  $hP5$ , and lattice parameters:  $a = 3.69 \text{ \AA}$ ,  $c = 5.83 \text{ \AA}$ ,  $z_U = 0.2467$ ,  
 77 and  $z_N = 0.6470$  [35, 36].  $\text{UN}_x$  has the fluorite crystal structure in the composition range  
 78 of  $1.75 \leq x \leq 2.00$ , whereas the  $\text{UN}_2/\alpha\text{-U}_2\text{N}_3$  solid solution is stable for  $1.54 \leq x \leq 1.75$   
 79 [31]. Additionally, the conventional unit cell of  $\alpha\text{-U}_2\text{N}_3$  can be regarded as a  $2 \times 2 \times 2$   
 80  $\text{UN}_2$  supercell with a quarter of the N atoms removed [37]. For these reasons, the names  
 81  $\text{UN}_2$  and  $\text{U}_2\text{N}_3$  are often used interchangeably to refer to the  $\text{UN}_2/\alpha\text{-U}_2\text{N}_3$  solid solution at  
 82 low and intermediate temperatures [31, 4]. The  $\text{UN}_2/\alpha\text{-U}_2\text{N}_3$  solid solution decomposes at a  
 83 temperature of either 1324 K [4] or 1405 K [38], the uncertainty being due to the dependence  
 84 of the U-N phase diagram on the nitrogen vapor pressure [4]. Due to the same uncertainty,  
 85  $\beta\text{-U}_2\text{N}_3$  exists as a single phase in either the temperature range 1324-1648 K [4] or the range  
 86 1214-1625 K [38].

87 We compare the UN lattice constant predicted by both potentials through 0 K energy  
 88 minimization to the experimental value. The UN linear thermal expansion coefficient (LTEC)  
 89 predicted by both potentials is also computed. To allow comparison with the Hayes *et al.*  
 90 [32] empirical correlation, the mean LTEC is defined as (assuming isotropic expansion):

$$\alpha_L = \frac{a - a_0}{a_0(T - T_0)} \quad (1)$$

91 where  $a$  is the lattice parameter and  $a_0$  is the lattice parameter at a reference temperature  
 92  $T_0 = 300 \text{ K}$ . It should be noted that this definition of the LTEC is different from the

93 thermodynamic definition:  $\alpha_L = (1/a)\partial a/\partial T$ . To calculate the temperature variation of the  
94 lattice parameters and LTECs of UN,  $\text{UN}_2$ ,  $\alpha$ - and  $\beta$ - $\text{U}_2\text{N}_3$ ,  $15 \times 15 \times 15$  supercells of UN,  
95  $\text{UN}_2$ , and  $\alpha$ - $\text{U}_2\text{N}_3$  (and  $8 \times 8 \times 8$  supercells of  $\beta$ - $\text{U}_2\text{N}_3$ ) are equilibrated in the *NPT* ensemble  
96 for 100 ps and their lattice parameters are averaged over the last 50 ps. Unless otherwise  
97 stated, these supercell sizes are used in all subsequent calculations.

98 *2.2. Melting point*

99 The thermodynamic definition of melting is the point at which solid and liquid states co-  
100 exist, and thus have the same free energy [39, 40]. However, the melting point predicted by  
101 MD based on simple heating corresponds to the point at which the solid lattice mechanically  
102 collapses, and is usually overestimated compared to the true one due to the existence of a free  
103 energy barrier to the formation of a solid-liquid interface in perfect supercells. This barrier  
104 leads to a hysteresis effect associated with the necessity to run the simulation for a sufficient  
105 time at a superheated temperature so that a seed of the liquid phase can spontaneously nu-  
106 cleate [41, 39]. This free-energy barrier can be eliminated by using the void-induced melting  
107 method [39, 40]. Voids (introduced in the supercell in the form of Schottky defects) form local  
108 pockets of a liquid-like structure, which effectively introduces solid-liquid interfaces. With  
109 increasing the number of voids, the free energy barrier to melting decreases, until, for a sufficient  
110 number of voids, the predicted melting point reaches a plateau for a limited range.  
111 If too many voids are introduced, the solid becomes mechanically unstable and collapses  
112 without a discontinuous solid-to-liquid phase transition [39]. Melting is a first-order phase  
113 transition that is signified by a step-like transition in the volume versus temperature curve,  
114 or, equivalently, a spike in the specific heat versus temperature curve [42]. Voids within the  
115 range 0-2 at. % are introduced into the UN supercells, which are then equilibrated in the  
116 *NPT* ensemble for 100 ps, their total energy and volume are averaged over the last 50 ps,  
117 and the solid-to-liquid transition temperatures are recorded for each void fraction.

118 *2.3. Elastic properties*

119 The elastic stiffness tensor,  $C_{ij}$ , is computed using the explicit deformation method [43].  
120 At 0 K, supercells of UN,  $\text{UN}_2$ ,  $\alpha$ - and  $\beta$ - $\text{U}_2\text{N}_3$  are relaxed and then strains are applied  
121 to the  $\pm x$ -,  $\pm y$ -, and  $\pm z$ -directions with magnitudes of 0.005%, 0.01%, and 0.05%. The  
122 supercell energy is minimized with a constant volume and the stress tensor is calculated.  
123 For the finite-temperature calculations, averaged UN and  $\text{UN}_2$  lattice parameters at each  
124 temperature are used to construct supercells of the same size, whereas, for  $\alpha$ - and  $\beta$ - $\text{U}_2\text{N}_3$ ,  
125 the supercells are initially equilibrated in the *NPT* ensemble for 50 ps. Supercells are then  
126 equilibrated for 20 ps using a Langevin thermostat, the Langevin thermostat is then switched  
127 off and strains of 0.5%, 0.1%, and 1.5% are applied to the same directions under the *NVE*  
128 ensemble. Finally, the stress tensor components are then averaged over the next 10 ps. For  
129 the UN,  $\text{UN}_2$ , and  $\alpha$ - $\text{U}_2\text{N}_3$  crystals with cubic symmetry, only three of the elastic constants  
130 are independent:  $C_{11}$ ,  $C_{12}$ , and  $C_{44}$  [44], whereas, for the hexagonal structure of  $\beta$ - $\text{U}_2\text{N}_3$ , five  
131 elastic constants are independent:  $C_{11}$ ,  $C_{12}$ ,  $C_{13}$ ,  $C_{33}$  and  $C_{44}$  [45]. Various strains are used  
132 at 0 K and finite temperatures to make sure the elastic properties are strain-independent.  
133 Larger strains are used at finite temperatures to reduce uncertainties arising from thermal  
134 fluctuations.

<sup>135</sup> Polycrystalline elastic moduli are computed from the single-crystal elastic constants ac-  
<sup>136</sup> cording to the Voigt-Reuss-Hill (VRH) approach [46, 44, 43] as Hill averages of upper Voigt  
<sup>137</sup> limits and lower Reuss limits on the bulk and shear moduli. The form of the VRH elastic  
<sup>138</sup> moduli is included in [Appendix A](#). The elastic stability criteria are also checked for UN, UN<sub>2</sub>,  
<sup>139</sup> and  $\alpha$ - and  $\beta$ -U<sub>2</sub>N<sub>3</sub>. For cubic crystals, the conditions for elastic stability are  $C_{11} - C_{12} > 0$ ,  
<sup>140</sup>  $C_{11} + 2C_{12} > 0$ , and  $C_{44} > 0$ , whereas, for hexagonal crystals, the elastic stability conditions  
<sup>141</sup> are:  $C_{11} > |C_{12}|$ ,  $2C_{13}^2 < C_{33}(C_{11} + C_{12})$ , and  $C_{44} > 0$  [47].

<sup>142</sup> The Anderson method is one of the standard methods to calculate the Debye temperature  
<sup>143</sup> from the 0 K elastic constants according to the equations [46]:

$$\theta_D = \frac{h}{k_B} \left( \frac{3q N_A \rho}{4\pi M} \right)^{1/3} v_0 \quad (2)$$

$$v_0 = \left[ \frac{1}{3} \left( \frac{2}{v_t^3} + \frac{1}{v_l^3} \right) \right]^{-1/3} \quad (3)$$

$$v_t = \sqrt{\frac{G}{\rho}} \quad (4)$$

$$v_l = \sqrt{\frac{3B + 4G}{3\rho}} \quad (5)$$

<sup>147</sup> where  $q$  is the number of atoms per formula unit ( $q = 2$  for UN),  $M$  is the molecular weight,  
<sup>148</sup>  $v_0$  is the average sound velocity,  $v_t$  is the average transverse sound velocity for an isotropic  
<sup>149</sup> material, and  $v_l$  is the average longitudinal sound velocity for an isotropic material. Another  
<sup>150</sup> method to calculate the Debye temperature for cubic crystals is the semi-empirical Siethoff-  
<sup>151</sup> Ahlborn method based on the room-temperature elastic constants [48]:

$$\theta_D = C \left( \frac{aqG'}{M} \right)^{1/2} \quad (6)$$

$$G' = \left[ C_{44} \left( \frac{(C_{11} - C_{12})C_{44}}{2} \right)^{1/2} \left( \frac{C_{11} - C_{12} + C_{44}}{3} \right) \right]^{1/3} \quad (7)$$

<sup>153</sup> where  $a$  is the lattice constant, and  $C$  is an empirical parameter that depends on the crystal  
<sup>154</sup> structure ( $C = 18.56$  K for the NaCl structure).  $q$  and  $M$  have the same meaning as in the  
<sup>155</sup> Anderson method. Both methods are utilized for the determination of  $\theta_D$  in this work.

#### <sup>156</sup> 2.4. Specific heat capacity

<sup>157</sup> Because UN behaves as a metallic solid [19, 49], its constant-pressure specific heat ca-  
<sup>158</sup> pacity,  $C_P$ , has two main contributions: lattice,  $C_{\text{lat}}$ , and electronic,  $C_{\text{elec}}$ , specific heat  
<sup>159</sup> capacities, where electron-phonon interactions have been neglected. To calculate  $C_{\text{lat}}$ , su-  
<sup>160</sup> percells are equilibrated in the  $NPT$  ensemble for 100 ps and their total energy is averaged  
<sup>161</sup> over the last 50 ps. All specific heats are computed as the slope of the potential energy as a

<sup>162</sup> function of temperature using three-point centered finite differences with 50 K increments.  
<sup>163</sup>  $C_{\text{lat}}$  can be decomposed into the following contributions [50, 51]:

$$C_{\text{lat}} = C_V + C_{\text{exp}} + C_{\text{anharm}} + C_d \quad (8)$$

<sup>164</sup> where  $C_V$  is the constant-volume specific heat,  $C_{\text{exp}}$  is the contribution due to thermal  
<sup>165</sup> expansion,  $C_{\text{anharm}}$  is the anharmonic non-expansive contribution, and  $C_d$  is the contribution  
<sup>166</sup> due to defect generation.  $C_V$  is calculated by restricting the supercells to the equilibrium 0  
<sup>167</sup> K volume and averaging the total energy within the  $NVT$  ensemble.  $C_{\text{exp}}$  can be calculated  
<sup>168</sup> from [52]:

$$C_{\text{exp}} = 9\alpha_L^2 BV_m T \quad (9)$$

<sup>169</sup> where  $\alpha_L$  is the linear thermal expansion coefficient,  $B$  is the bulk modulus, and  $V_m$  is the  
<sup>170</sup> molar volume. Neglecting  $C_d$  for perfect crystals,  $C_{\text{anharm}}$  (Fig. 4d) is calculated from:

$$C_{\text{anharm}} = C_{\text{lat}} - C_V - C_{\text{exp}} \quad (10)$$

<sup>171</sup>  $C_{\text{elec}}$  is estimated from [53, 20, 49]:

$$C_{\text{elec}} = \frac{\pi}{3} g(\epsilon_F) N_A k_B^2 T = \gamma T \quad (11)$$

<sup>172</sup> where  $g(\epsilon_F)$  is the density of states (DOS) at the Fermi level (states/eV-atom), and  $\gamma$  is the  
<sup>173</sup> electronic specific heat coefficient ( $\text{J/mol-K}^2$ ). Samsel-Czekala *et al.* [6] reported a value of  $\gamma$   
<sup>174</sup> = 3.7 mJ/mol-K<sup>2</sup> based on their electronic-structure calculation, and this is the value used in  
<sup>175</sup> our calculations. Kocevski *et al.* [49] reported  $g(\epsilon_F)$  = 2-2.2 states/eV-atom in their *ab initio*  
<sup>176</sup> MD calculation, which gives a value of  $\gamma$  equal to about 1.5-1.7 mJ/mol-K<sup>2</sup>. These  $\gamma$  values  
<sup>177</sup> are in large contrast with the experimentally reported values of about 34 mJ/mol-K<sup>2</sup> [54]  
<sup>178</sup> and 50 mJ/mol-K<sup>2</sup> [55] obtained by fitting heat capacity data. Szpunar *et al.* [56] have also  
<sup>179</sup> calculated  $\gamma$  using the Quantum ESPRESSO code and found  $\gamma$  = 17.6 mJ/mol-K<sup>2</sup> for the  
<sup>180</sup> PBEsol functional and  $\gamma$  = 0.6 mJ/mol-K<sup>2</sup> for the non-local hybrid B3LYP functional—both  
<sup>181</sup> values being smaller than the experimental ones.

## <sup>182</sup> 2.5. Phonon properties

<sup>183</sup> To get a deeper understanding of the calculated thermal properties of UN, we study how  
<sup>184</sup> the Tseplyaev and Kocevski potentials model the UN phonon properties. Harmonic force  
<sup>185</sup> constants are calculated using the finite displacement method [57]. To compute accurate  
<sup>186</sup> forces using small displacements, initial UN structures must be fully relaxed [58], which was  
<sup>187</sup> accomplished using static energy minimization in LAMMPS. The equilibrium UN lattice  
<sup>188</sup> constants of each potential are then used to construct  $3 \times 3 \times 3$  UN *primitive* cells (54  
<sup>189</sup> atoms). PhonoLAMMPS, coupled to LAMMPS, is used to apply a displacement of 0.01 Å  
<sup>190</sup> to the supercell and get the interatomic forces of the displaced configurations, where the  
<sup>191</sup> required displacement patterns are determined by the symmetry of the supercell. Phonopy  
<sup>192</sup> reads the generated forces and calculates symmetrized harmonic force constants from [59, 60]:

$$K_{ls\alpha, l's'\beta} = -\frac{\partial F_{ls\alpha}}{\partial u_{l's'\beta}} \quad (12)$$

where  $K_{l\alpha,l's'\beta}$  is a second-order (harmonic) force constant,  $l$  labels the unit cells,  $s$  labels the atoms within each unit cell,  $\alpha$  and  $\beta$  label Cartesian coordinates,  $u_{l's'\beta}$  is the displacement of atom  $s'$  within unit cell  $l'$  in the  $\beta$  direction and the force  $F_{l\alpha} = -\partial U / \partial u_{l\alpha}$  where  $U$  is the lattice potential energy. The phonon band structure is calculated along the high symmetry  $k$ -path:  $\Gamma-X-K-\Gamma-L$  to allow comparison with experimental results. To compute the phonon DOS, the reciprocal space is sampled by a  $\Gamma$ -centered  $100 \times 100 \times 100$  mesh, and the linear tetrahedron method is used for integration in the Brillouin zone.

## 2.6. Point defect formation energies

The formation energy of uncharged point defects at  $T = 0$  K is defined as [61, 62, 63]:

$$E_f = E_d - E_p - \sum_i n_i \mu_i = \delta E - \sum_i n_i \mu_i \quad (13)$$

where  $E_d$  and  $E_p$  are the energies of the defective and perfect supercells, respectively,  $n_i$  is the number of atoms of type  $i$  removed ( $n_i < 0$ ) or added ( $n_i > 0$ ) to form the defect, and  $\mu_i$  is the chemical potential of the  $i$ th species.  $\delta E$  is termed the “raw” formation energy [61]. For Schottky defects (SD) and Frenkel defects (FD), the crystal’s stoichiometry does not change, and special cases of Eq. (13) exist. For Frenkel defects, the formation energy is just  $E_f = E_d - E_p$ , whereas, for a Schottky defect, the formation energy is:

$$E_f = E_d - \frac{N - A}{N} E_p \quad (14)$$

where  $N$  is the total number of atoms in the supercell, and  $A$  is the number of atoms per formula unit ( $A = 2$  for UN) [64].

Chemical potentials represent the energy of the reservoirs with which atoms are being exchanged [62, 65], and the proper choice of the chemical potentials in Eq. (13) depends on phase stabilities of the considered system [65]. For a binary compound AB, the chemical potentials of A and B vary from A-rich to B-rich compositions displaying a discontinuity at the stoichiometric composition [66, 61, 67]. While numerous formalisms exist in the literature for determining the chemical potentials of relevant species [61, 13, 66, 67, 62, 27], the method of Huang *et al.* [68, 19] is used in this work. In this method, upper and lower bounds are imposed on the chemical potential to capture its dependence on stoichiometry; these bounds are dictated by the cohesive energies of the competing phases at very low temperatures. Based on an examination of the UN phase diagram [38, 4], it can be argued that the bounds on the U and N chemical potentials at very low temperatures are governed by transformations to  $\alpha$ -U for U-rich conditions (i.e., co-existence of UN and  $\alpha$ -U), and transformation to  $\text{UN}_2$  for N-rich conditions (i.e., co-existence of UN and  $\text{UN}_2$ ) [68, 19]. Accordingly, the U and N chemical potentials are calculated from [19]:

$$E_c(\text{U}_x\text{N}_y) = x\mu_{\text{U}} + y\mu_{\text{N}} \quad (15)$$

where  $E_c(\text{U}_x\text{N}_y)$  is the cohesive energy (energy per formula unit). Eq. (15) is solved for UN and  $\alpha$ -U to get the U-rich chemical potentials, and for UN and  $\text{UN}_2$  to get the N-rich chemical potentials [68, 19]. The chemical potentials at stoichiometric conditions are the averages of these two bounds [67].

228 Although many DFT studies have investigated point defect formation energies in UN  
 229 [11, 13, 14, 24, 25, 27], only Yang and Kaltsoyannis [19] and Kocevski *et al.* [10] have looked  
 230 at their variation with stoichiometry. Yang and Kaltsoyannis used the PW91 functional,  
 231 whereas Kocevski *et al.* used the PBE and AM05 functionals, with and without an added  
 232 on-site Coulomb repulsion term ( $+U$ ), and found a variation of the defect formation energies  
 233 with different DFT methodologies.

### 234 3. Results

#### 235 3.1. Structural properties

236 The UN lattice parameters predicted by the Tseplyaev and Kocevski potentials at 0 K  
 237 are 4.81 Å and 4.90 Å, respectively, compared to the experimental room temperature (RT)  
 238 value of 4.89 Å [32]. As can be seen in Fig. 1a, the Kocevski potential is closer in comparison  
 239 to the empirical correlation of the UN lattice parameter, whereas the Tseplyaev potential  
 240 slightly underestimates it. The linear thermal expansion coefficient (LTEC) is shown in  
 241 Fig. 1b. The Tseplyaev potential predicts a temperature-independent thermal expansion up  
 242 to about 1000 K and then predicts a fifth-order power-law expansion—a trend that does not  
 243 agree with experimental observations, while the Kocevski potential underestimates the UN  
 244 LTEC with a larger error than that of the Tseplyaev potential, but predicts nearly the same  
 245 trend as a function of temperature observed in experiments.

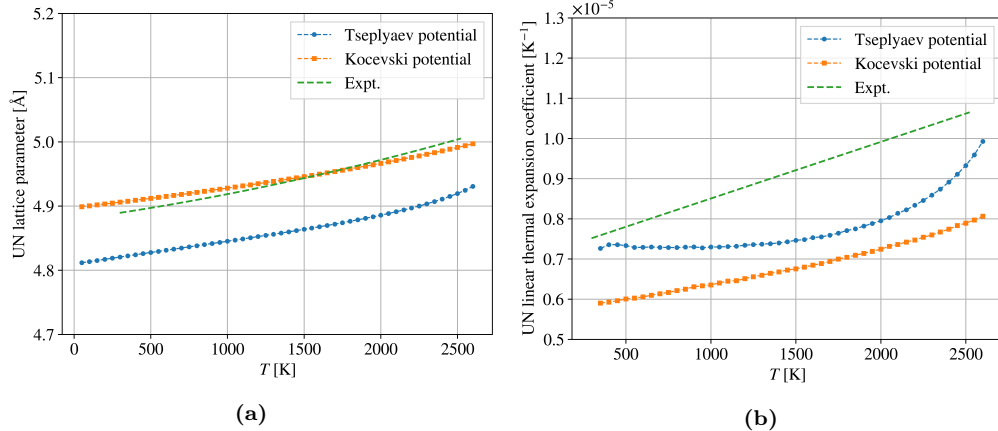


**Figure 1:** (a) UN lattice parameter calculated by both potentials and compared to the empirical correlation of Hayes *et al.* (1990) [32]. (b) UN linear thermal expansion coefficient calculated by both potentials and compared to the experimental data of Hayes *et al.* (1990) [32].

#### 246 3.2. Melting point

247 The melting temperature predicted by both potentials is shown in Fig. 2. According to  
 248 Alavi and Thompson [39], the thermodynamic melting point is determined as the value of  
 249 the range over which the melting temperature appears to be independent of the void fraction.  
 250 Based on this measure, the Tseplyaev potential predicts thermodynamic melting at about  
 251 2700 K, whereas the Kocevski potential predicts it at about 3100 K; a value that is close to  
 252 the experimental value of 3035 K estimated from the Hayes *et al.* correlation at a nitrogen

vapor pressure of 1 atm [33]. It can be concluded that the Kocevski potential gives a better prediction of the phase stability range of UN because its predicted melting point is closer to the experimental data, whereas the Tseplyaev potential predicts a slightly premature melting of UN.

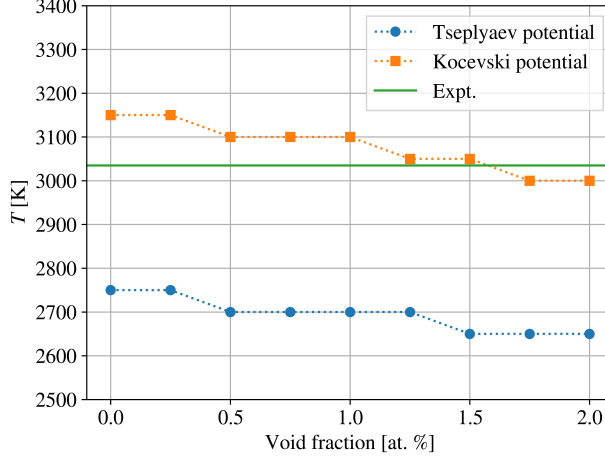


**Figure 2:** UN melting point as predicted by both potentials as a function of void fraction using the void-induced melting method. The experimental melting temperature (3035 K) is taken from the Hayes *et al.* correlation at a nitrogen vapor pressure of 1 atm [33].

### 3.3. Elastic properties

The UN elastic constants calculated at 0 K using both potentials are shown in Table 1. A much larger error is associated with the values of  $C_{11}$  and  $C_{44}$  calculated by the Tseplyaev potential compared to those calculated by the Kocevski potential, whereas the Tseplyaev potential estimation of  $C_{12}$  is slightly better. It was found that UN elastic constants calculated at 0 K using the Tseplyaev potential show a discontinuity compared to finite-temperature values, which contradicts the third law of thermodynamics that requires a near-zero slope of the elastic constants versus  $T$  curves as  $T$  approaches 0 K [69]. This discontinuity can be attributed to static energy minimization predicting metastable states of strained UN supercells. Thermal motion is likely to lead the strained supercells to a global minimum of the potential energy hypersurface. For this reason, we also compute the elastic constants at 1 K. The elastic constants, moduli, and Poisson's ratio at finite temperatures are shown in Fig. 3. When calculated by the Kocevski potential, 1 K elastic constants show no significant difference from those calculated at 0 K, whereas 1 K elastic constants calculated by the Tseplyaev potential led to the disappearance of the discontinuity. All computed elastic constants were found to be independent of the amount of strain within the computational uncertainty.

In Fig. 3a,  $C_{12}$  and  $C_{44}$  computed by the Tseplyaev potential show a good agreement with experimental values at RT, whereas it overestimates RT  $C_{11}$  by more than 35%. On the other hand, all elastic constants calculated by the Kocevski potential agree well with the experimental values at RT. Regarding the elastic moduli (Fig. 3b), the Tseplyaev potential reproduces the experimental Young's modulus by Hayes *et al.* [71] at RT, while the RT value calculated by the Kocevski potential can be regarded as an average estimate of the

**Table 1:** UN elastic constants (GPa) as calculated by both potentials. Experimental elastic constants are at 290 K.

	$C_{11}$	$C_{12}$	$C_{44}$	$B$
Tseplyaev potential (0 K)	586.6	110.5	54.7	269.2
Tseplyaev potential (1 K)	602.1	125.5	54.9	284.4
Kocevski potential (0 K)	425.4	117.0	71.0	219.8
Expt. [70]	423.9	98.1	75.7	206.7

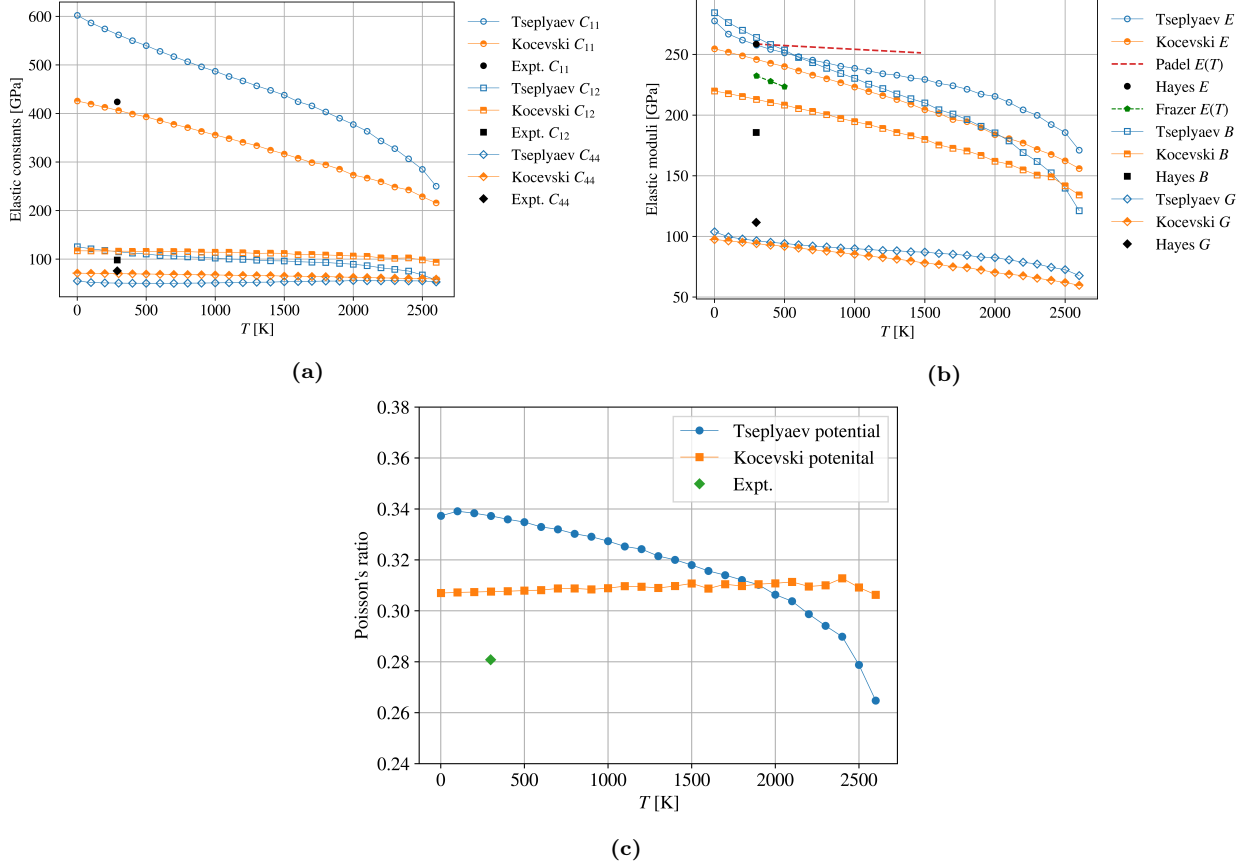


**Figure 3:** Computations of the temperature variation of (a) UN elastic constants,  $C_{11}$ ,  $C_{12}$ , and  $C_{44}$ , (b) UN Young's modulus,  $E$ , bulk modulus,  $B$ , and shear modulus,  $G$ , and (c) Poisson's ratio as calculated by both potentials. The experimental data points in (a) are from Salleh *et al.* (1986) [70]. The experimental data points in (b) and (c) are from Hayes *et al.* (1990) [71]. The experimental variation of Young's modulus with temperature in (b) is due to Padel and de Novion [72], which Hayes *et al.* assumed to be valid also for UN's bulk and shear moduli, and due to the more recent study by Frazer *et al.* [73].

value of Hayes *et al.* [71] and Frazer *et al.* [73]. The Tseplyaev potential overestimates the UN bulk modulus by more than 40%, whereas the Kocevski potential shows a better prediction and only overestimates it by about 15%. Both potentials slightly underestimate the shear modulus,  $G$ . The Kocevski potential shows a good prediction of the UN Poisson's ratio compared to the experimental value at RT (Fig. 3c) and predicts a slight increase with increasing temperature, which is the expected trend. However, the Tseplyaev potential predicts a decrease of the Poisson's ratio with increasing temperature, related to the significant

286 softening of the bulk modulus.

287 The only experimental measurements of the temperature variation of the UN elastic  
288 properties are the studies by Padel and de Novion [72] and by Frazer *et al.* [73] on the tem-  
289 perature dependence of UN Young's modulus. Padel and de Novion [72] report a temperature  
290 dependence of Young's modulus of the form:

$$E(T) = E_0 (1 - 2.375 \times 10^{-5}T) \quad (16)$$

291 in the temperature range of 298-1473 K, with no experimental data to support it, whereas  
292 Frazer *et al.* predict a dependence of the form:

$$E(T) = 245.78 - 0.0449T \quad (17)$$

293 in the temperature range of 300-500 K.

294 Eq. (16) predicts a softening rate that is much slower than that predicted by either  
295 potential as is obvious in Fig. 3b, whereas, despite its limited range, the softening rate implied  
296 by Frazer *et al.*'s data [73] seems to agree better with that predicted by both potentials. Hayes  
297 *et al.* [71] assumed the temperature dependence of Eq. (16) applies for all elastic properties  
298 except for Poisson's ratio, which they assumed to be independent of temperature. This  
299 latter assumption agrees with Poisson's ratio calculated by the Kocevski potential which  
300 can be approximated as temperature-independent. Kocevski *et al.* [27] also calculated the  
301 temperature variation of the UN elastic properties using their potential. Our results generally  
302 agree with theirs for all elastic properties except for Poisson's ratio which they estimated  
303 to be  $\sim 0.22$  at RT compared to the experimental value of  $\sim 0.28$  and our value of 0.31.  
304 The reason for this discrepancy is that they calculated Poisson's ratio from the formula:  
305  $\nu = C_{12}/(C_{11} + C_{12})$ , which assumes the elastic constants are of an isotropic material which  
306 is not the case for UN, as  $C_{11} - C_{12} \neq 2C_{44}$  [70, 74].

307 The computed Debye temperatures using different methods are given in Table 2 and  
308 compared to values reported in the literature. Values calculated in this work fall within the  
309 range 355-368 K and agree with the values calculated by Scarbrough *et al.* [55] and Whaley  
310 *et al.* [75]. A large scatter is evident in the experimental Debye temperature values which  
311 range from 181-364 K. Scarbrough *et al.* [55] suspected that the values reported by Counsell  
312 *et al.* [54] and Westrum and Barber [76] (276 K and 289 K, respectively) are likely affected  
313 by the presence of magnetic specific heat. Salleh *et al.* [70] report a value of  $\theta_D = 282$  K  
314 without any reference to the method they used to derive it. It's interesting to note that when  
315 Salleh *et al.*'s RT elastic constants are substituted into the Anderson and Siethoff-Ahlborn  
316 methods, they give values of  $\theta_D = 365$  K and  $\theta_D = 373$  K, respectively.

317 Baranov *et al.* [77] made a mistake in their estimation of the Debye temperature. They  
318 computed the Debye frequency using  $\omega_D = v_0 k_D$ , where  $v_0$  is the average phonon group  
319 velocity estimated from Eq. (3) with  $v_0 = 2990$  m/s (given that  $v_l = 4740$  m/s and  $v_t =$   
320  $2691$  m/s) and  $k_D = (6\pi^2/\Omega)^{1/3}$ , where  $\Omega$ , the volume of the primitive UN unit cell, is equal  
321 to  $a^3/4$ ,  $a$  being the lattice parameter [78]. Instead of using the volume of the *primitive* UN  
322 unit cell, they used the volume of the conventional unit cell, which led to an underestimation  
323 of the Debye temperature  $\theta_D = \hbar\omega_D/k_B$ . Instead of  $\theta_D = 181$  K, their appropriate value  
324 should have been  $\theta_D = 289$  K. Interestingly, when using the formula  $v_0 = (v_l + 2v_t)/3$  to  
325 average the velocities of the acoustic branches [78],  $v_0 = 3373$  m/s and Baranov *et al.*'s

**Table 2:** UN Debye temperature values estimated in this work and reported in the literature.

Method	Reference	$\theta_D$
Tseplyaev potential + Anderson method	This work	365 K
Tseplyaev potential + Siethoff-Ahlborn method	This work	356 K
Kocevski potential + Anderson method	This work	355 K
Kocevski potential + Siethoff-Ahlborn method	This work	356 K
Sound-velocity measurements in polycrystalline UN	Whaley <i>et al.</i> [75]	361-364 K
Specific heat measurements in the temperature range 1.3-4.6 K	Scarborough <i>et al.</i> [55]	324 K
Specific heat measurements in the temperature range 5-350 K	Westrum and Barber [76]	289 K
Specific heat measurements in the temperature range 11-320 K	Counsell <i>et al.</i> [54]	276 K
Not reported	Salleh <i>et al.</i> [70]	282 K
Derived from the UN phonon spectrum measured at 4.2 K	Baranov <i>et al.</i> [77]	181 K
DFT calculation	Mei <i>et al.</i> [9]	244 K

326  $\theta_D = 326$  K, which is close to our calculated values. Based on this analysis, it can be  
327 concluded that the variation of the experimental Debye temperature between the two ranges  
328 276-289 K and 324-365 K can partly be attributed to the differences in the averaging formulas  
329 used to estimate the average acoustic phonon group velocity. Another contribution is the  
330 antiferromagnetic nature of UN which leads the  $\theta_D$  estimated from specific heat data to  
331 be smaller than that estimated from elastic constants as pointed out by Whaley *et al.* [75].  
332 Based on this analysis, we can conclude that the average UN  $\theta_D$  is around 362 K as estimated  
333 from both experimental and computed elastic constants.

### 334 3.4. Specific heat capacity

335 UN  $C_P$  and its components are shown in Fig. 4.  $C_{\text{exp}}$  (Fig. 4c) is calculated from functions  
336 fitted to the UN LTEC (Eqs. (B.1) and (B.2)) and bulk modulus (Eqs. (B.3) and (B.4)), and  
337  $C_{\text{anharm}}$  (Fig. 4d) is calculated from functions fitted to the values of  $C_P$  (Eqs. (B.5) and (B.6))  
338 and  $C_V$  (Eqs. (B.7) and (B.8)) calculated by both potentials. It can be seen in Fig. 4a that  
339 the Tseplyaev potential compares well with the UN  $C_P$  experimental correlation from Hayes  
340 *et al.* [33]. However, care must be taken when comparing to the high-temperature values of  
341 this correlation as discussed by Galvin *et al.* [79]. Both potentials agree in the computed  $C_P$   
342 and  $C_V$  up to about 1200 K and 700 K, respectively, whereas at higher temperatures, the  
343 Kocevski potential significantly underestimates both  $C_P$  and  $C_V$ . The Tseplyaev potential  
344 predicts that the anharmonic contribution is nearly zero at low and intermediate tempera-  
345 tures, and only becomes significant at  $T > 1800$  K, whereas the Kocevski potential predicts  
346 a minor contribution across the entire temperature spectrum. As can be seen in Fig. 4,  
347 the discrepancy between the  $C_P$  computed by both potentials ( $\sim 30$  J/mol-K at 2500 K)  
348 can almost completely be attributed to a difference in the computed  $C_V$  ( $\sim 10$  J/mol-K at  
349 2500 K) and a difference in the estimated  $C_{\text{anharm}}$  ( $\sim 20$  J/mol-K at 2500 K), whereas the  
350 difference in the thermal expansion contribution is quite small ( $\sim 1$  J/mol-K at 2500 K). It is  
351 interesting to note that the structural inaccuracies of the Tseplyaev potential in determining  
352 both the bulk modulus and the LTEC nearly balance and cancel out giving a  $C_{\text{exp}}$  value  
353 that is very close to that predicted by the Kocevski potential at low temperatures. That is,  
354 the Tseplyaev-potential predictions of UN properties are energetically accurate despite the  
355 observed structural and elastic inaccuracies.

356       $C_V$  and  $C_{\text{anharm}}$  are completely determined by the phonon properties of the material,  
 357      and, thus, to understand why the Kocevski potential underestimates the UN  $C_P$ , a deeper  
 358      investigation of the UN phonon properties as predicted by both potentials is necessary and  
 359      will be shown in Section 3.5.

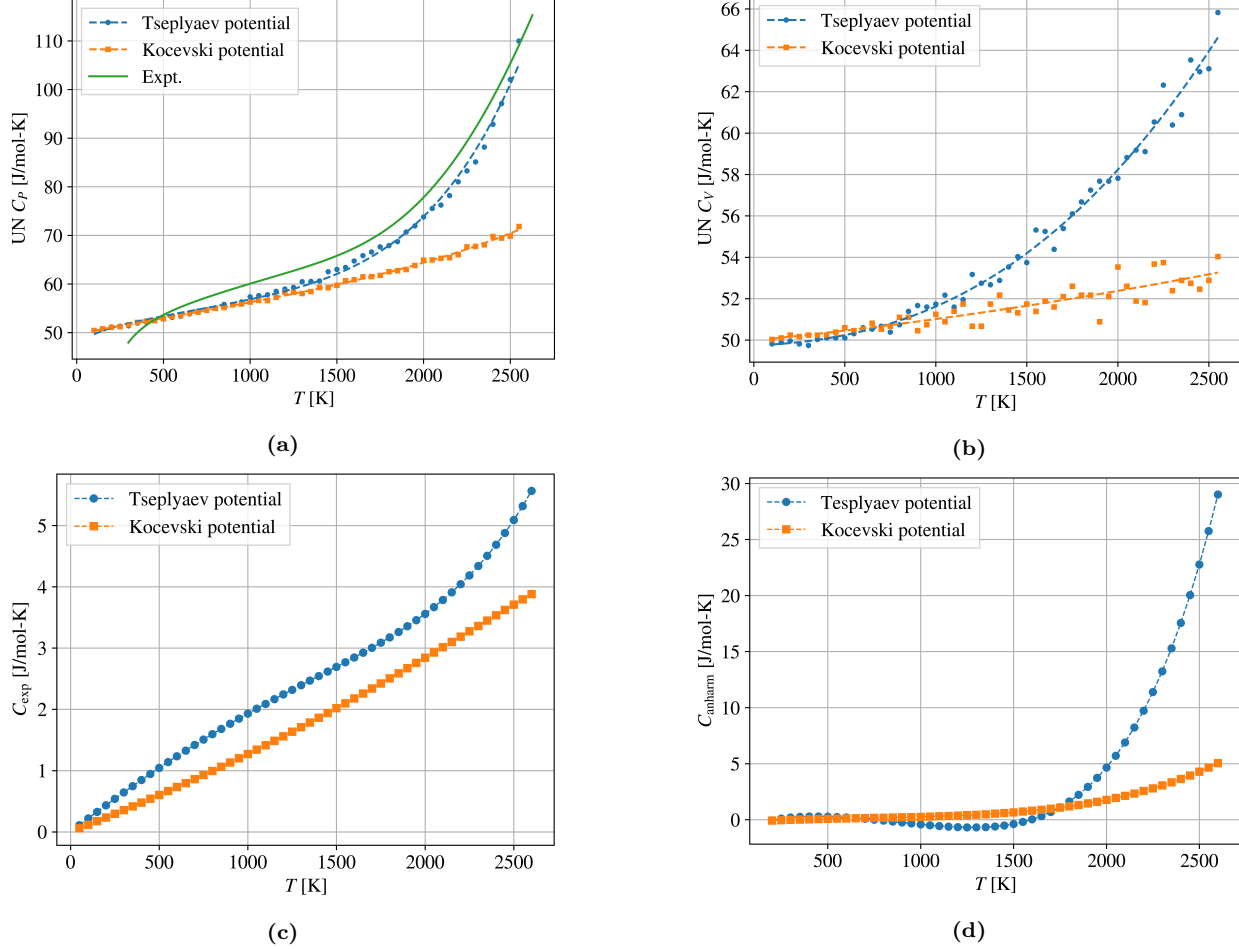


**Figure 4:** (a)  $C_P$  and (b)  $C_V$  of UN as calculated by both potentials and compared to the empirical correlation of Hayes *et al.* (1990) [33]. (c) The thermal expansion contribution to the specific heat. (d) The anharmonic non-expansive contribution to the specific heat.

### 360      3.5. Phonon properties

361      The results for the UN phonon properties are shown in Fig. 5. Experimental data for UN  
 362      phonon band structure and density of states (DOS) were measured by Jackman *et al.* [80] and  
 363      Aczel *et al.* [81] at temperatures of 4.2 K and 5 K, respectively. Given that anharmonicity  
 364      should be negligible at these cryogenic temperatures, we have carried out phonon calculations  
 365      in the harmonic approximation for comparison. It can be observed from the phonon band  
 366      structure (Fig. 5a) and phonon DOS (Fig. 5b) that both potentials show a good qualitative  
 367      agreement with the experimentally observed acoustic phonon spectrum while overestimating  
 368      the acoustic phonon DOS. It can also be seen in Fig. 5a that the Tseplyaev potential  
 369      only predicts the upper portion of the optical phonon spectrum with moderate qualitative

370 agreement, whereas it completely misses the lower optical branches. The optical branches  
 371 predicted by the Tseplyaev potential coincide only for some portion of the  $k$ -path because the  
 372 potential lacks the long-range electrostatic interaction, which is responsible for splitting the  
 373 longitudinal and transverse optical phonon branches in ionic materials [82]. Fig. 5b shows  
 374 that the optical phonon frequency range predicted by the Kocevski potential is overestimated  
 375 by about 1.9 THz compared to experimental measurements, incorrectly describing all optical  
 376 branches.

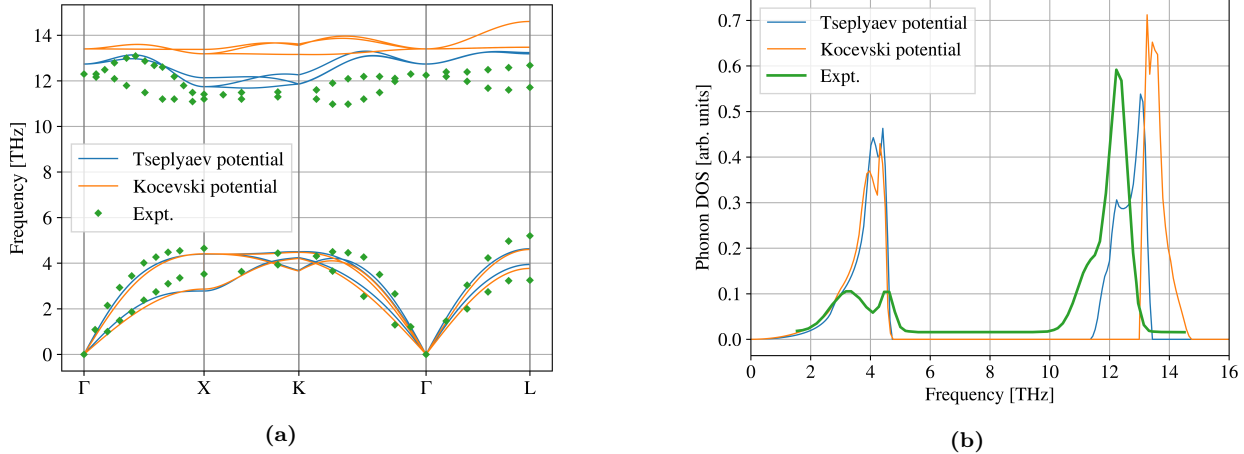


**Figure 5:** (a) UN phonon band structure as calculated by both potentials and compared to the experimental data of Jackman *et al.* [80]. (b) UN phonon density of states (DOS) as calculated by both potentials and compared to the inelastic neutron scattering data of Aczel *et al.* [81]. The areas under the phonon DOS plots have been normalized to 1 to allow comparison between calculations and the experiment.

377 The acoustic phonon spectrum and low-frequency DOS are related to the vibrations of  
 378 the heavier uranium atoms, whereas the optical phonon spectrum and high-frequency DOS  
 379 are related to the vibrations of the lighter nitrogen atoms [77, 45]. Therefore, it can be  
 380 concluded that both potentials accurately model the uranium atom vibrations whereas only  
 381 the Tseplyaev potential can qualitatively model the nitrogen atom vibrations. From these  
 382 results, the Kocevski potential underestimation of the UN  $C_P$  compared to that predicted  
 383 by the Tseplyaev potential can be attributed to the Kocevski potential overestimation of  
 384 the optical phonon frequency range. The contribution of the optical phonons to the specific  
 385 heat can be treated by the Einstein model. Due to their nearly flat dispersion curve, optical  
 386 phonons are approximated within the Einstein model as having a single average frequency,  
 387  $\omega_E$ , independent of  $k$ . From the experimental UN dispersion curve,  $\omega_E = 12.0$  THz, whereas  
 388  $\omega_E = 12.5$  THz for the Tseplyaev potential, and  $\omega_E = 13.9$  THz for the Kocevski potential.  
 389 Because phonons are bosons, they follow the Bose-Einstein distribution [45]:

$$f_{BE} = \frac{1}{\exp(\hbar\omega/k_B T) - 1} \quad (18)$$

390 where  $f_{BE}$  quantifies the mean number of phonons of frequency  $\omega$  present in thermal equi-  
 391 librium at temperature  $T$  [83]. With the Kocevski potential overestimating  $\omega_E$ , it predicts  
 392 a smaller average number of excited optical phonons, which leads to a smaller contribution  
 393 of the optical phonons to the UN specific heat. Torres *et al.* [58] also observed the same

trend while analyzing the phonon properties predicted by existing  $\text{UO}_2$  empirical potentials. By including both harmonic and higher-order force constants in their phonon calculations, they found that  $\text{UO}_2$  empirical potentials that overestimate the 0 K optical phonon frequency range tend to underestimate the specific heat, especially at near-melting temperatures. Zhou *et al.* [82] also made a similar observation about the Stillinger-Weber potential of GaN, and attributed its underestimation of the specific heat at high temperatures to the overestimated optical phonon range. The Debye temperature quantifies the temperature above which all phonon modes become excited and below which some phonon modes freeze out [83]. Based on our analysis in Section 3.3,  $\theta_D$  is around 362 K, which means that even at temperatures near RT we can expect optical phonons to contribute to the UN specific heat. Baranov *et al.* [77] also noted that due to the ionic character of the UN chemical bond, optical phonons are expected to predominate the oscillation spectrum of the UN lattice at temperatures above  $\theta_D$ .

The agreement between the lattice thermal conductivity predicted by Galvin *et al.* [79] using both potentials despite the discrepancy of the predicted specific heats can be understood if we note that the two potentials predict the same acoustic phonon spectrum and DOS at 0 K. For bulk materials, the thermal conductivity is largely dictated by acoustic phonons because they are the main heat carriers [84]. In contrast, the contribution of optical phonons to the thermal conductivity of bulk materials is very small due to their short lifetimes and low group velocities [85].

### 3.6. Point defect formation energies

Perfect  $6 \times 6 \times 6$  supercells of UN were energy-minimized at 0 K using the conjugate gradient algorithm implemented in LAMMPS. A fractional energy tolerance of  $1 \times 10^{-9}$  was used allowing volume change. For the Tseplyaev potential, we used energy tolerances in the range  $10^{-6}$ - $10^{-15}$  and found that the raw formation energies of the defective supercells vary by several eV with decreasing the energy tolerance down to a tolerance of  $10^{-9}$  at which the raw formation energy becomes somewhat insensitive to the energy tolerance. This is indicative of the complex potential energy surface predicted by the Tseplyaev potential and the likely existence of several metastable states. This strong dependence of the raw formation energy on energy tolerance was not observed for the Kocevski potential. The cohesive energies of UN,  $\alpha$ -U, and  $\text{UN}_2$  and chemical potentials were calculated for both potentials and are shown in Tables B.7 and B.8. It should be noted that the Kocevski potential predicts positive cohesive energy for  $\alpha$ -U (i.e., it cannot predict a stable  $\alpha$ -U phase), which would lead to unphysical chemical potentials and incorrect formation energies for the U-rich and stoichiometric conditions. For this reason, point defects under U-rich and stoichiometric conditions are not considered for the Kocevski potential in this work.

For the 0 K calculations, point defects were then introduced into  $6 \times 6 \times 6$  UN supercells. U and N interstitials were inserted only in cubic interstitial sites. Yang and Kaltsoyannis [19] have observed that when a U Frenkel defect is introduced within a UN supercell, it is annihilated by the tiny atomic movements of the relaxation process. To prevent this phenomenon, the initial forces on all inserted interstitials were set to zero. Defective supercells were relaxed using the same procedure used for the perfect supercells.

To avoid the possibility of defective supercells converging to metastable energy states by static minimization at 0 K, the 0 K formation energies are averaged over many defect

438 configurations, and, additionally, the formation energies are also calculated at 1 K.  $8 \times 8 \times 8$   
 439 supercells of UN are equilibrated in the *NPT* ensemble for 50 ps, where the system's potential  
 440 energy is averaged over the last 20 ps. Point defects are inserted in the equilibrated UN  
 441 supercells, and the defective system is allowed to evolve under the *NPT* ensemble for 50 ps  
 442 where the system's potential energy is also averaged over the last 20 ps. The calculation is  
 443 repeated using five unique initial velocity distributions, utilizing the average potential energy  
 444 of this sample to obtain defect energetics. Chemical potentials and formation energies are  
 445 calculated using the same procedure employed at 0 K. The Tseplyaev potential is also used to  
 446 calculate the finite-temperature formation enthalpy for U FD, N FD, and SD with 15 unique  
 447 initial velocity distributions in the temperature range of 100-1500 K. The 1500 K limit is  
 448 chosen because in UN diffusion begins to be experimentally observed at this temperature  
 449 [86]. Thus, at and beyond 1500 K, the measured raw formation enthalpies would be affected  
 450 by defect migration.

**Table 3:** Formation energies (eV) for stoichiometric point defects. FD stands for Frenkel defect, and SD stands for Schottky defect. A semi-bonded SD is composed of two vacancies at (0, 0, 0) and (0.5, 0.5, 0.5).

	Tseplyaev potential		Kocevski potential		DFT
	0 K	1 K	0 K	1 K	
Unbonded U FD	9.32	8.02	14.41	14.30	9.46 [19], 6.31-10.19 [10]
Bonded U FD	7.26	-	10.3	-	-
Unbonded N FD	4.67	4.50	4.03	4.00	4.90-5.04 [19], 4.43-4.95 [10]
Bonded N FD	3.76	-	3.23	-	-
Unbonded SD	4.57	4.52	3.98	3.88	4.96-5.15 [19], 4.25-5.47 [10]
Semi-bonded SD	4.51	-	3.99	-	-
Bonded SD (divacancy)	4.35	-	3.04	-	4.17 [19]

**Table 4:** Formation energies (eV) for non-stoichiometric point defects. Standard Kröger-Vink notation [87] has been used for point defects but with charges omitted due to the inability of MD to simulate charged defects.

	U-rich		Stoichiometric		N-rich						
	Tseplyaev 0 K	1 K	DFT	Tseplyaev 0 K	1 K	DFT	Kocevski 0 K	1 K	DFT		
$V_U$	3.45	3.33	3.17-3.43 [19], 3.27-3.86 [10]	2.19	2.14	2.75-3.01 [19]	0.93	0.95	0.60	0.54	2.34-2.60 [19], 2.09-2.58 [10]
$V_N$	1.11	1.29	1.76-1.90 [19], 0.62-1.86 [10]	2.37	2.48	2.18-2.31 [19]	3.62	3.67	3.35	3.34	2.59-2.72 [19], 1.42-2.82 [10]
$U_i$	6.43	3.99	2.81-6.33 [10]	7.69	5.18	-	8.95	6.37	13.82	13.76	3.79-7.78 [10]
$N_i$	3.73	3.21	2.96-3.82 [10]	2.47	2.02	-	1.21	0.83	0.89	0.66	2.00-3.01 [10]
$U_N$	1.61	1.86	1.74-3.16 [10]	4.13	4.24	-	6.65	6.62	18.32	15.90	3.72-5.52 [10]
$N_U$	9.32	5.84	5.99-7.67 [10]	6.80	3.46	-	4.28	1.08	4.71	1.70	4.06-5.19 [10]

451 The calculated formation energies are reported in [Tables 3](#) and [4](#). Bonded SD and FD  
 452 are formed by introducing the two vacancies, and the vacancy and interstitial, respectively,  
 453 within the same unit cell, whereas unbonded SD and FD are formed by introducing the two  
 454 vacancies, and the vacancy and interstitial, respectively, within different unit cells. Dashes  
 455 in [Table 3](#) for bonded defects at 1 K indicate that these defects relaxed to the defect-free  
 456 crystal structure. The formation energy of the N FD is slightly higher than the formation  
 457 energies of the unbonded SD and divacancy due to the lattice's compact structure which  
 458 offers limited room for an interstitial. The formation energies predicted by the Tseplyaev  
 459 potential at 0 K and 1 K are generally consistent with each other except for the values  
 460 predicted for unbonded U FD,  $U_i$ , and  $N_U$  which show differences in the range 1.30-3.48 eV,  
 461 with the 0 K values being generally larger than the 1 K values. This is because calculating

462 the formation energies at 1 K using the Tseplyaev potential allows us to approach the ground  
 463 state of the defect structure, whereas the calculation at 0 K fails to do so. This is especially  
 464 true for  $U_i$ , whose most stable configuration in UN is reported as the dumbbell configuration  
 465 [24], whereas, by visual inspection of the  $U_i$  structure at 0 K (not shown),  $U_i$  still resides  
 466 at the cubic interstitial site after static minimization using the Tseplyaev potential. The  
 467 difference in  $U_i$  formation energy between 0 K and 1 K also explains the difference in the  
 468 formation energy of U FD. This discrepancy most likely signifies that the Tseplyaev potential  
 469 predicts metastable states for the defected UN supercells at 0 K, a situation that we also  
 470 encountered with strained UN supercells at 0 K. Thus, caution should be exercised when  
 471 utilizing or examining 0 K defect properties calculated by the Tseplyaev potential. The  
 472 formation energies predicted by the Tseplyaev potential generally show excellent agreement  
 473 with the DFT-predicted values for U-rich, N-rich, and stoichiometric conditions. The Ko-  
 474 cevski potential predicts formation energies for N FD and SD in agreement with DFT, but  
 475 it overestimates the U FD defect by more than 4 eV. As explained previously, the Kocevski  
 476 potential cannot predict formation energies for U-rich and stoichiometric conditions due to  
 477 the inability to describe metallic U. However, for N-rich conditions, the formation energies  
 478 predicted by the Kocevski potential qualitatively agree with DFT-values for most defects  
 479 except for  $U_i$  and  $U_N$ , which are overestimated by a factor of 2-3. It can be concluded  
 480 that the Tseplyaev potential shows a better performance in the calculation of point defect  
 481 formation energy, whereas the Kocevski potential is only suitable for stoichiometric point  
 482 defects. It can also be concluded that in U-rich conditions,  $V_N$  and  $U_N$  accommodate most  
 483 of the off-stoichiometry, whereas, in N-rich conditions,  $V_U$  and  $N_i$  accommodate most of the  
 484 off-stoichiometry.

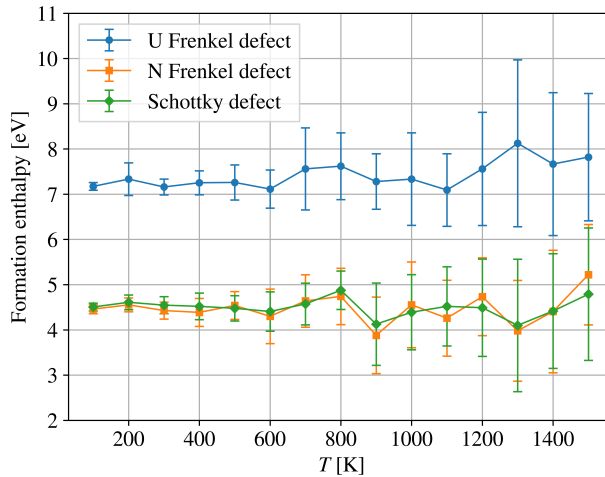


**Figure 6:** Defect formation enthalpy as a function of temperature for the U Frenkel defect, N Frenkel defect, and Schottky defect in UN as a function of temperature as calculated by the Tseplyaev potential. Error bars correspond to one standard deviation.

485 Formation enthalpies of U FD, N FD, and SD in UN as a function of temperature are  
 486 shown in Fig. 6. As expected, the standard deviation increases with increasing temperature.  
 487 The average formation enthalpy of U FD is confined to about 7-8 eV, whereas those of N  
 488 FD and SD are confined to about 4-5 eV, with no apparent dependence on temperature.

489 3.7.  $UN_2$ ,  $\alpha$ - $U_2N_3$  and  $\beta$ - $U_2N_3$

490 3.7.1. Thermophysical properties

491 The  $UN_2$  lattice parameter and  $C_P$  predicted by both potentials are shown in Figs. 7a  
 492 and 7b, respectively. The Tseplyaev potential gives a better prediction of the  $UN_2$  lattice  
 493 parameter with a slight underestimation and predicts a phase transition at about 800 K. On  
 494 the other hand, the Kocevski potential overestimates the  $UN_2$  lattice parameter and predicts  
 495 a stable  $UN_2$  structure up to 1400 K. It should be noted that the phase transition temperature  
 496 of  $UN_2$  is 1324–1405 K [4, 38]. It is also worth mentioning that Silva *et al.* [31] reported  
 497 lattice constants of  $UN_2$  and  $\alpha$ - $U_2N_3$  as a function of temperature; however, their samples  
 498 were not of high purity but rather included the  $UN_2/\alpha$ - $U_2N_3$  solid solution, and, thus, are  
 499 not ideal for comparison. The Tseplyaev potential overestimates the  $UN_2 C_P$  compared to  
 500 that calculated by the Kocevski potential, a trend that was also observed for UN. Due to  
 501 the lack of experimental measurements, we compare the predicted  $C_P$  with the Dulong–Petit  
 502 value which, for a compound, is defined as  $3nR$ ,  $n$  being the number of atoms per formula  
 503 unit ( $n = 3$  for  $UN_2$ , and  $n = 5$  for  $\alpha$ - and  $\beta$ - $U_2N_3$ ), and  $R$  being the gas constant [88]. The  
 504 Dulong–Petit value serves as a theoretical lower limit on  $C_P$  data for solids well above room  
 505 temperature and is useful to compare against in the absence of experimental measurements.  
 506 The  $UN_2 C_P$  predicted by both potentials approach the Dulong–Petit value around room  
 507 temperature and deviate from it at higher temperatures, which is the theoretically expected  
 508 trend.

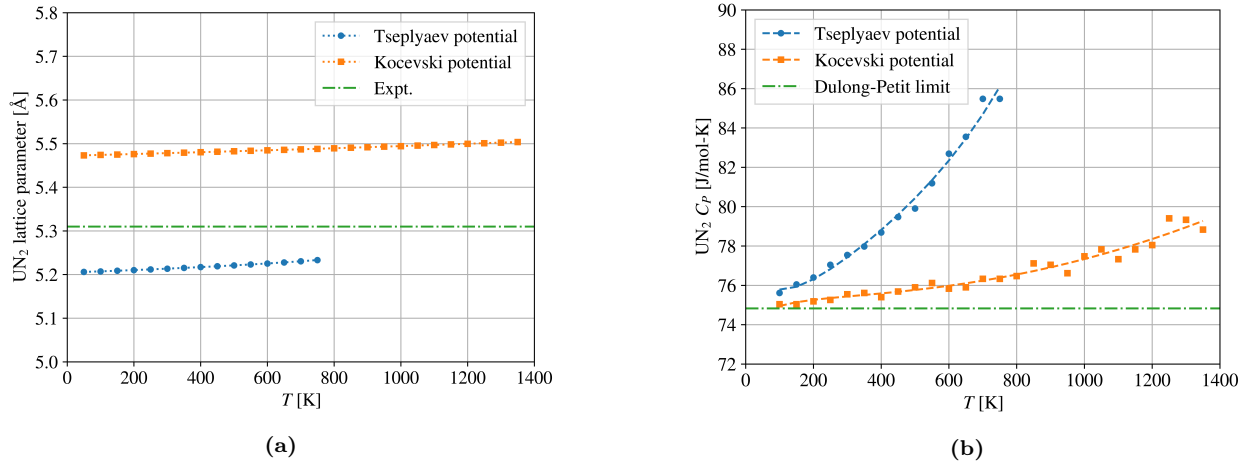


**Figure 7:** (a) The lattice parameter of  $UN_2$  calculated by both potentials as a function of temperature. (b)  $UN_2 C_P$  calculated by both potentials as a function of temperature.  $C_P$  calculated by the Tseplyaev and Kocevski potentials are fitted to Eqs. (B.9) and (B.10), respectively. The experimental lattice parameter of  $UN_2$  is taken from Lu *et al.* [89] and included as a horizontal line because the temperature at which it was measured is not reported.

509 The Tseplyaev potential could not predict a stable structure above 0 K for either  $\alpha$ - $U_2N_3$   
 510 or  $\beta$ - $U_2N_3$ , so we only discuss the finite temperature  $\alpha$ - and  $\beta$ - $U_2N_3$  properties predicted by  
 511 the Kocevski potential (Fig. B.11). The Kocevski potential predicts that the  $\alpha$ - $U_2N_3$  phase  
 512 is mechanically stable up to about 1000 K. For  $\alpha$ - $U_2N_3$ , the Kocevski potential overestimates  
 513 the lattice parameter, and for  $\beta$ - $U_2N_3$ , it overestimates the  $a$  parameter and underestimates

the  $c$  parameter. The  $\alpha$ - and  $\beta$ - $\text{U}_2\text{N}_3$   $C_P$  predicted by the Kocevski potential nearly coincide and approach the Dulong–Petit value around RT. Additionally, the Kocevski potential predicts that the  $\beta$ - $\text{U}_2\text{N}_3$  structure can be mechanically stable at very low temperatures.

As mentioned earlier, the Tseplyaev potential is a modified version of the ADP developed by Kuskin *et al.* [24]. The authors reported that Kuksin’s potential could stabilize the structures of  $\alpha$ - and  $\beta$ - $\text{U}_2\text{N}_3$ . However, Tseplyaev and Starikov [25] don’t report any capability of the modified version of the potential to simulate polymorphs of  $\text{U}_2\text{N}_3$  at zero pressure. Thus, it appears that in the modification of the potential to improve UN property prediction, the capability was lost for other phases in the U-N system.

### 3.7.2. Elastic properties

The 0 K elastic constants of  $\text{UN}_2$  are shown in Table 5. The predictions of the Kocevski potential show a good agreement with the DFT predictions for  $C_{12}$  and  $C_{44}$ , whereas it underestimates  $C_{11}$  by about 40%. The predictions of the Tseplyaev potential show much larger errors: it overestimates  $C_{11}$  and  $C_{12}$  by more than 70%, and 40%, respectively, and its  $C_{44}$  value is overestimated by nearly a factor of 5. The temperature dependence of the  $\text{UN}_2$  elastic constants and moduli are shown in Fig. 8. The Kocevski potential shows general qualitative agreement with the  $\text{UN}_2$  elastic moduli predicted by DFT, whereas the Tseplyaev potential greatly overestimates all elastic moduli and fails to give qualitative predictions. The Kocevski potential shows minimal softening of the  $\text{UN}_2$  elastic properties with increasing temperature.

**Table 5:**  $\text{UN}_2$  elastic constants (GPa) at 0 K as calculated by both potentials. The DFT values are from Lu *et al.* [89] and have been calculated using the GGA+ $U$  approach with  $U = 2$  eV.

	$C_{11}$	$C_{12}$	$C_{44}$
Tseplyaev potential	856.2	201.4	291.7
Kocevski potential	275.9	184.1	67.8
DFT [89]	488.2	140.5	55.3

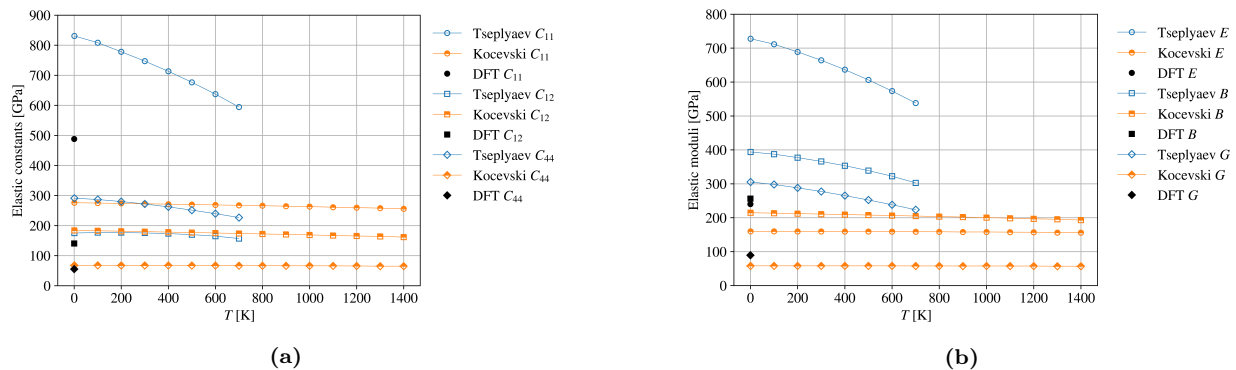


**Figure 8:** The predicted temperature variation of (a)  $\text{UN}_2$  elastic constants,  $C_{11}$ ,  $C_{12}$ , and  $C_{44}$ , (b)  $\text{UN}_2$  Young’s modulus,  $E$ , bulk modulus,  $B$ , and shear modulus,  $G$ . The DFT values are from Lu *et al.* [89].

The 0 K elastic constants of  $\alpha$ - $\text{U}_2\text{N}_3$  calculated by the Kocevski potential are  $C_{11} = 185.4$  GPa,  $C_{22} = 141.8$  GPa, and  $C_{44} = 41.8$  GPa, whereas the elastic constants and moduli calculated at finite temperatures are shown in Figs. 9a and 9b, respectively. To the

best of our knowledge, no experimental or DFT elastic property data exist for  $\alpha\text{-U}_2\text{N}_3$ . It can be observed that  $\alpha\text{-U}_2\text{N}_3$  is generally softer than  $\text{UN}_2$  which is expected because, as explained earlier, the  $\alpha\text{-U}_2\text{N}_3$  conventional unit cell lacks 16 N atoms, and thus has fewer bonds compared to the  $2 \times 2 \times 2$   $\text{UN}_2$  supercell.

For  $\beta\text{-U}_2\text{N}_3$ , the 0 K elastic constants are shown in [Table 6](#). The predictions of both potentials satisfy the stability criteria of the hexagonal lattice and nearly agree, except for  $C_{33}$  which the Tseplyaev potential overpredicts by a factor of 23, and  $C_{44}$  which the Tseplyaev potential underestimates with an error of about 50%—all relative to the values predicted by the Kocevski potential at 0 K. The bulk modulus predicted by the Kocevski potential agrees perfectly with that predicted by the DFT study of Lu *et al.* [89]. The elastic constants and bulk modulus of  $\beta\text{-U}_2\text{N}_3$  predicted by the Tseplyaev potential vary significantly by varying the strain, whereas those predicted by the Kocevski potential show a negligible dependence on the strain value. This is indicative of potential instabilities using the Tseplyaev potential for  $\beta\text{-U}_2\text{N}_3$ , which are confirmed through the evaluation of the structure at finite temperatures, which decomposes as discussed. The variation of the  $\beta\text{-U}_2\text{N}_3$  elastic constants with temperature is shown in [Fig. 10a](#).  $C_{11}$  and  $C_{33}$  show observable softening,  $C_{12}$  shows a slower softening rate, and  $C_{13}$  and  $C_{44}$  are nearly constant.  $\beta\text{-U}_2\text{N}_3$  elastic moduli are shown in [Fig. 10b](#). As explained earlier, the predicted bulk modulus qualitatively agrees with DFT values. In general, further experimental investigations are required to validate the predicted properties of  $\text{UN}_2$ ,  $\alpha\text{-U}_2\text{N}_3$ , and  $\beta\text{-U}_2\text{N}_3$ .

**Table 6:**  $\beta\text{-U}_2\text{N}_3$  elastic properties (GPa) as calculated by both potentials.  $B = 232$  GPa has been calculated by Evarestov *et al.* [7] using the LCAO DFT approach.  $B = 209.2$  GPa has been calculated by Lu *et al.* [89] using the GGA+ $U$  approach with  $U = 2$  eV.

	$C_{11}$	$C_{12}$	$C_{13}$	$C_{33}$	$C_{44}$	$B$
Tseplyaev potential	372.4	166.8	118.1	5680.1	30.0	534.5
Kocevski potential	357.0	224.2	140.7	242.7	64.5	210.0
DFT						232 [7], 209.2 [89]

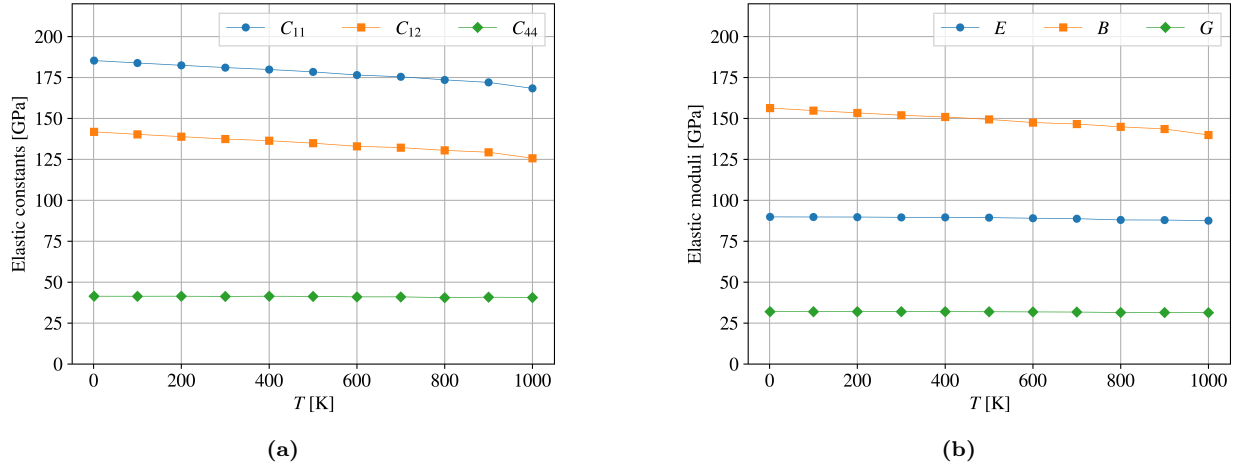


**Figure 9:** (a) Elastic constants,  $C_{11}$ ,  $C_{12}$ , and  $C_{44}$ , (b) Young's modulus,  $E$ , bulk modulus,  $B$ , and shear modulus,  $G$ , of  $\alpha\text{-U}_2\text{N}_3$  as calculated by the Kocevski potential.

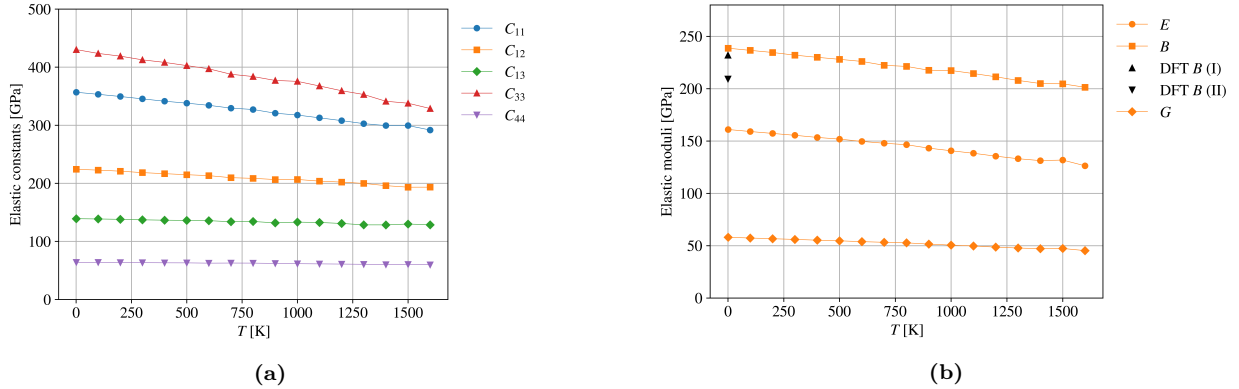


**Figure 10:** (a) Elastic constants,  $C_{11}$ ,  $C_{12}$ ,  $C_{13}$ ,  $C_{33}$ , and  $C_{44}$ , (b) Young's modulus,  $E$ , bulk modulus,  $B$ , and shear modulus,  $G$ , of  $\beta$ -U<sub>2</sub>N<sub>3</sub> as calculated by the Kocevski potential. DFT  $B$  (I) is from Evarestov *et al.* [7] and DFT  $B$  (II) is from Lu *et al.* [89].

#### 557 4. Discussion

558 Based on the presented results, we can identify several features of both potentials. In  
 559 general, the Kocevski potential shows better predictability of the structural aspects of UN,  
 560 e.g., lattice parameter and elastic properties as a function of temperature, whereas the  
 561 Tseplyaev potential better predicts the UN energetic aspects, e.g., the specific heat and  
 562 defect formation energies. One drawback of the Kocevski potential is the overestimation  
 563 of the UN optical phonon range, leading to its underestimation of the UN  $C_P$ , compared  
 564 to the Hayes *et al.* [33] correlation, at temperatures greater than 1200 K. Moreover, the  
 565 Kocevski potential cannot predict a stable metallic  $\alpha$ -U structure. Therefore, its applicability  
 566 to studies related to UN non-stoichiometry is limited. The Tseplyaev potential does an  
 567 inferior job of predicting the UN elastic properties and underpredicts the experimental lattice  
 568 parameter values compared to the Kocevski potential. The Tseplyaev potential predicts with  
 569 reasonable accuracy the UN phonon band structure, although the predicted optical branches  
 570 coincide near the  $\Gamma$ -point due to the absence of long-range electrostatic interactions in the  
 571 ADP model. The relative accuracy of the phonon behavior predicted by the Tseplyaev  
 572 potential should make it preferable in the evaluation of thermal conductivities. Another  
 573 important feature of the Tseplyaev potential is that it predicts metastable states for defected  
 574 UN supercells at 0 K, and thus we recommend avoiding its usage at 0 K. Thus, each potential  
 575 has realms of applicability for the description of the UN system, and the noted drawbacks  
 576 must be acknowledged when deciding which potential to utilize.

577 The predictions of UN<sub>2</sub> properties by the Kocevski potential show better qualitative  
 578 agreement with the limited experimental and DFT values; however, neither potential pro-  
 579 duces results with a satisfactory level of accuracy. The Tseplyaev potential cannot predict  
 580 stable structures for  $\alpha$ - and  $\beta$ -U<sub>2</sub>N<sub>3</sub> and predicts premature phase change of both UN and  
 581 UN<sub>2</sub>. Thus, the Tseplyaev potential is not suitable for studies related to the stability of  
 582 different uranium nitride phases. On the other hand, the Kocevski potential predicts stable  
 583  $\alpha$ - and  $\beta$ -U<sub>2</sub>N<sub>3</sub> structures with reasonable lattice parameters, reasonably predicts the melt-  
 584 ing point of UN and predicts a mechanical stability range of UN<sub>2</sub> closer to that represented  
 585 by the U-N system phase diagrams. This makes the Kocevski potential the best option for

586 studies involving many uranium nitride phases, although more experimental data are needed  
587 to further assess its predictions of UN<sub>2</sub>, and  $\alpha$ - and  $\beta$ -U<sub>2</sub>N<sub>3</sub> properties.

588 Areas of importance that have not been assessed in this study include the dynamical  
589 processes of plastic deformation, i.e., dislocation formation and slip, interfacial properties,  
590 and radiation damage. Such analyses are beyond the scope of this work, but potential com-  
591 parison and validation should be conducted before utilization of either potential to explore  
592 these phenomena.

## 593 5. Conclusions

594 This work aimed to evaluate two UN interatomic potentials: Tseplyaev and Starikov's  
595 ADP [25] and Kocevski *et al.*'s EAM potential [27]. The study involved assessing the pre-  
596 dictive capabilities of these potentials for various thermophysical and elastic properties of  
597 UN, UN<sub>2</sub>, and  $\alpha$ - and  $\beta$ -U<sub>2</sub>N<sub>3</sub>. The Kocevski potential underestimates the UN specific heat  
598 which is attributed to its overestimation of the UN optical phonon frequency range. In  
599 terms of performance, the Tseplyaev potential excels in capturing the energetic aspects of  
600 UN, whereas the Kocevski potential performs better in modeling the UN's structural prop-  
601 erties. Regarding the mechanical stability of phases, the Kocevski potential demonstrates  
602 superior predictive capabilities, in that it can reasonably estimate the UN melting point  
603 and predicts stable  $\alpha$ - and  $\beta$ -U<sub>2</sub>N<sub>3</sub> structures. In contrast, the Tseplyaev potential predicts  
604 premature phase changes for both UN and UN<sub>2</sub> and fails to stabilize either polymorph of  
605 U<sub>2</sub>N<sub>3</sub>. An important limitation of the Kocevski potential is its inability to predict a stable  
606 metallic U phase, making it unsuitable for studies related to UN non-stoichiometry.

## 607 Acknowledgements

608 The authors would like to thank Antoine Claisse for the fruitful discussions. Mohamed  
609 AbdulHameed dedicates this work to the memory of Abu Bakr Etman. This research made  
610 use of the resources of the High-Performance Computing Center at Idaho National Labora-  
611 tory, which is supported by the Office of Nuclear Energy of the U.S. Department of Energy  
612 and the Nuclear Science User Facilities under Contract No. DE-AC07-05ID14517.

## 613 Appendix A. Voigt-Reuss-Hill elastic moduli

614 For an isotropic polycrystalline material with a cubic crystal structure, the form of the  
615 VRH elastic moduli is [46, 90]:

$$B = B_V = B_R = \frac{C_{11} + 2C_{12}}{3} \quad (\text{A.1})$$

$$G_V = \frac{C_{11} - C_{12} + 3C_{44}}{5} \quad (\text{A.2})$$

$$G_R = \frac{5C_{44}(C_{11} - C_{12})}{4C_{44} + 3(C_{11} - C_{12})} \quad (\text{A.3})$$

$$G = \frac{G_V + G_R}{2} \quad (\text{A.4})$$

$$E = \frac{9BG}{3B + G} \quad (\text{A.5})$$

$$\nu = \frac{3B - 2G}{6B + 2G} \quad (\text{A.6})$$

616 For the  $\beta\text{-U}_2\text{N}_3$  hexagonal crystal, the Voigt and Reuss limits on the bulk and shear  
 617 moduli are formulated in terms of the components of both the stiffness tensor,  $C_{ij}$ , and the  
 618 compliance tensor,  $S_{ij}$  [46, 91]:

$$B_V = \frac{2C_{11} + 2C_{12} + 4C_{13} + C_{33}}{9} \quad (\text{A.7})$$

$$B_R = \frac{1}{2S_{11} + 2S_{12} + 4S_{13} + S_{33}} \quad (\text{A.8})$$

$$B = \frac{B_V + B_R}{2} \quad (\text{A.9})$$

$$G_V = \frac{2C_{11} - C_{12} - 2C_{13} + C_{33} + 6C_{44} + 3C_{66}}{15} \quad (\text{A.10})$$

$$G_R = \frac{15}{8S_{11} - 4S_{12} - 8S_{13} + 4S_{33} + 6S_{44} + 3S_{66}} \quad (\text{A.11})$$

623 where  $S_{11}$ ,  $S_{12}$ ,  $S_{13}$ ,  $S_{33}$ , and  $S_{44}$  are the independent components of the compliance tensor,  
 624 and:

$$S_{11} = \frac{C_{11}C_{33} - C_{13}^2}{C_{11}(C_{11}C_{33} - 2C_{13}^2) - C_{12}(C_{12}C_{33} + 2C_{13}^2)} \quad (\text{A.12})$$

$$S_{12} = \frac{-C_{12}C_{33} + C_{13}^2}{C_{11}(C_{11}C_{33} - 2C_{13}^2) - C_{12}(C_{12}C_{33} + 2C_{13}^2)} \quad (\text{A.13})$$

$$S_{13} = \frac{-C_{13}}{C_{33}(C_{11} + C_{12}) - 2C_{13}^2} \quad (\text{A.14})$$

$$S_{33} = \frac{C_{11} + C_{12}}{C_{33}(C_{11} + C_{12}) - 2C_{13}^2} \quad (\text{A.15})$$

$$S_{44} = \frac{1}{C_{44}} \quad (\text{A.16})$$

$$C_{66} = \frac{C_{11} - C_{12}}{2} \quad (\text{A.17})$$

$$S_{66} = 2(S_{11} - S_{12}) \quad (\text{A.18})$$

<sup>631</sup> **Appendix B. Supplementary information**

<sup>632</sup> In all equations presented in this appendix, the superscript  $T$  refers to the Tseplyaev  
<sup>633</sup> potential and the superscript  $K$  refers to the Kocevski potential.

<sup>634</sup> The temperature variation of the LTEC computed by both potentials is fitted to the  
<sup>635</sup> following functions:

$$\alpha_L^T = 7.321 \times 10^{-6} - 3.063 \times 10^{-11}T + 2.154 \times 10^{23}T^5 \quad (R^2 = 99.8\%) \quad (\text{B.1})$$

$$\alpha_L^K = 5.773 \times 10^{-6} + 3.866 \times 10^{-10}T + 1.813 \times 10^{-13}T^2 \quad (R^2 = 99.9\%) \quad (\text{B.2})$$

<sup>637</sup> in the temperature range 50-2500 K.

<sup>638</sup> The temperature dependence of the bulk modulus computed by both potentials is fitted  
<sup>639</sup> to the following quadratic functions:

$$B^T = 275.063 - 3.314 \times 10^{-2}T - 7.649 \times 10^{-6}T^2 \quad (R^2 = 98.4\%) \quad (\text{B.3})$$

$$B^K = 219.196 - 1.955 \times 10^{-2}T - 4.517 \times 10^{-6}T^2 \quad (R^2 = 99.8\%) \quad (\text{B.4})$$

<sup>641</sup> in the temperature range of 1-2600 K.

<sup>642</sup> The UN  $C_P$  and  $C_V$  computed by both potentials have been fitted to:

$$C_P^T = 61.612 + 4.709 \times 10^{-3}T + 3.754 \times 10^{-16}T^5 - 19.663/T^{0.1} \quad (R^2 = 99.4\%) \quad (\text{B.5})$$

$$C_P^K = 50.500 + 6.193 \times 10^{-3}T + 1.272 \times 10^{-13}T^4 - 1.140/T^{0.1} \quad (R^2 = 99.7\%) \quad (\text{B.6})$$

$$C_V^T = 49.341 + 7.144 \times 10^{-4}T + 4.016 \times 10^{-8}T^{2.5} + 0.591/T^{0.1} \quad (R^2 = 98.8\%) \quad (\text{B.7})$$

$$C_V^K = 49.978 + 8.757 \times 10^{-4}T + 1.616 \times 10^{-7}T^2 \quad (R^2 = 80.8\%) \quad (\text{B.8})$$

<sup>643</sup> The UN<sub>2</sub>  $C_P$  calculated by both potentials are fitted to:

$$C_P^T = 54.894 + 1.803 \times 10^{-2}T + 8.717 \times 10^{-15}T^5 + 30.248/T^{0.1} \quad (R^2 = 98.9\%) \quad (\text{B.9})$$

$$C_P^K = 82.060 - 2.445 \times 10^{-3}T + 3.199 \times 10^{-6}T^2 - 10.934/T^{0.1} \quad (R^2 = 95.1\%) \quad (\text{B.10})$$

<sup>644</sup> whereas the  $\alpha$ -U<sub>2</sub>N<sub>3</sub>  $C_P$  calculated by the Kocevski potential is fitted to:

$$C_P^K = 155.092 - 1.686 \times 10^{-2}T + 1.534 \times 10^{-5}T^2 - 45.235/T^{0.1} \quad (R^2 = 93.3\%) \quad (\text{B.11})$$

<sup>645</sup> and the  $\beta$ -U<sub>2</sub>N<sub>3</sub>  $C_P$  calculated by the Kocevski potential is fitted to:

$$C_P^K = 132.240 + 7.979 \times 10^{-4}T + 2.544 \times 10^{-6}T^2 - 11.483/T^{0.1} \quad (R^2 = 91.1\%) \quad (\text{B.12})$$

**Table B.7:** Cohesive energies (eV) of UN,  $\alpha$ -U and  $\text{UN}_2$ .

	Tseplyaev potential	Kocevski potential	Reference value
UN	-16.18	-13.02	-13.6 (Expt.) [7]
$\alpha$ -U	-5.23 (0 K); -5.37 (1 K)	-	-5.55 (Expt.) [92]
$\text{UN}_2$	-24.62	-22.18	-21.5 to -17.9 (DFT) [7]

**Table B.8:** U and N chemical potentials (eV) for different stoichiometric conditions.

	Tseplyaev potential			Kocevski potential
	U-rich	Stoichiometric	N-rich	N-rich
$\mu_U$	-5.23 (0 K); -5.37 (1 K)	-6.49 (0 K); -6.56 (1 K)	-7.75	-3.86
$\mu_N$	-10.95 (0 K); -10.81 (1 K)	-9.69 (0 K); -9.62 (1 K)	-8.43	-9.16

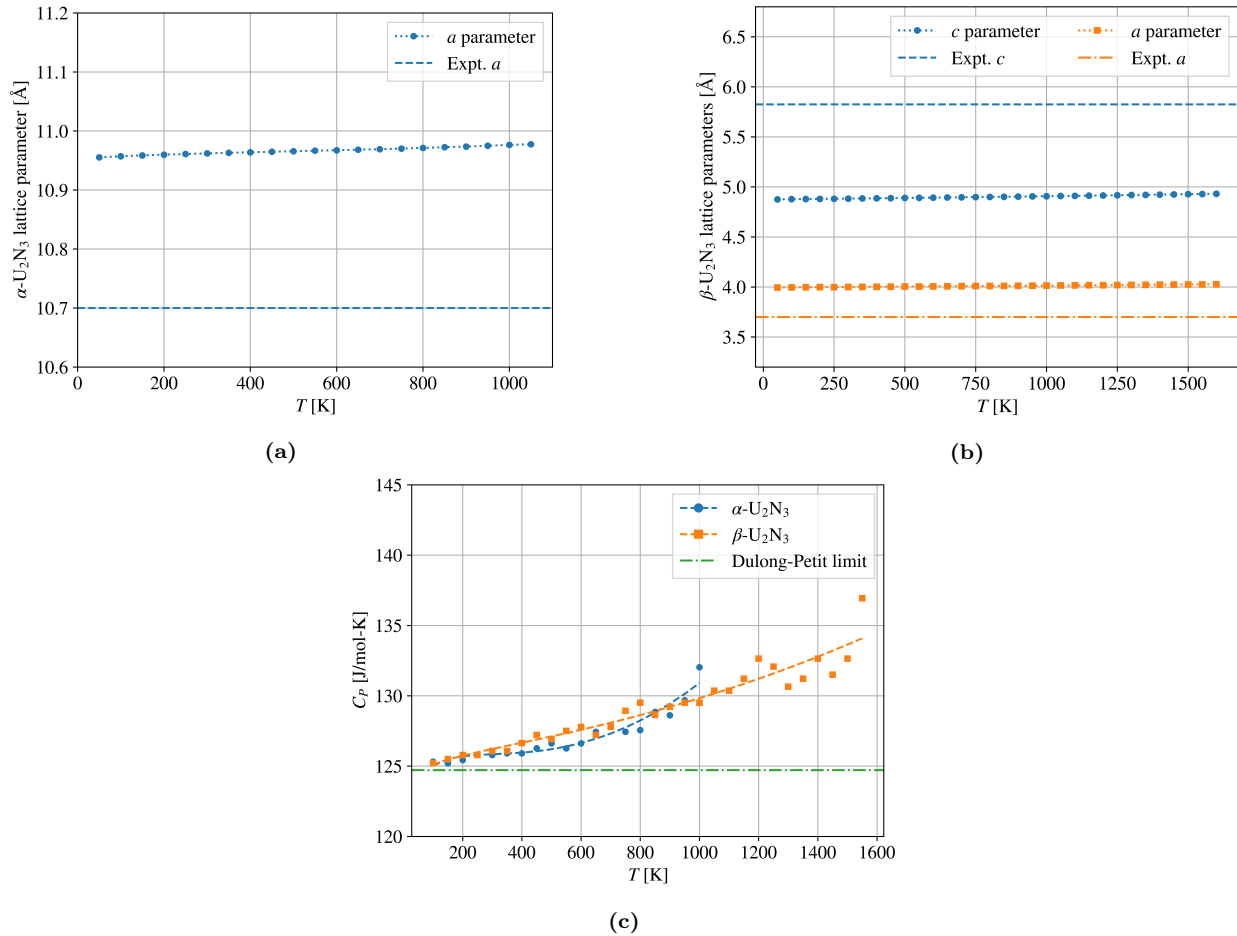


**Figure B.11:** The lattice parameters of (a)  $\alpha$ -U<sub>2</sub>N<sub>3</sub>, and (b)  $\beta$ -U<sub>2</sub>N<sub>3</sub> as calculated by the Kocevski potential. (c) The specific heats of  $\alpha$ - and  $\beta$ -U<sub>2</sub>N<sub>3</sub> as calculated by the Kocevski potential. The curve fit of  $C_P$  of  $\alpha$ - and  $\beta$ -U<sub>2</sub>N<sub>3</sub> as functions of temperature are given in Eqs. (B.11) and (B.12).

## 646 References

- 647 [1] J. K. Watkins, A. Gonzales, A. R. Wagner, E. S. Sooby, B. J. Jaques, Challenges  
648 and opportunities to alloyed and composite fuel architectures to mitigate high uranium

- 649 density fuel oxidation: Uranium mononitride, Journal of Nuclear Materials 553 (2021).  
650 [doi:10.1016/j.jnucmat.2021.153048](https://doi.org/10.1016/j.jnucmat.2021.153048).
- 651 [2] C. Ekberg, D. R. Costa, M. Hedberg, M. Jolkonen, Nitride fuel for Gen IV nuclear  
652 power systems, Journal of Radioanalytical and Nuclear Chemistry 318 (2018) 1713–  
653 1725. [doi:10.1007/s10967-018-6316-0](https://doi.org/10.1007/s10967-018-6316-0).
- 654 [3] J. Wallenius, Nitride fuels, Comprehensive Nuclear Materials 5 (2020) 88–101. [doi:10.1016/B978-0-12-803581-8.11694-7](https://doi.org/10.1016/B978-0-12-803581-8.11694-7).
- 655 [4] M. Uno, T. Nishi, M. Takano, Thermodynamic and thermophysical properties of  
656 the actinide nitrides, Comprehensive Nuclear Materials: Second Edition (2020) 202–  
657 231[doi:10.1016/B978-0-12-803581-8.11749-7](https://doi.org/10.1016/B978-0-12-803581-8.11749-7).
- 658 [5] A. Casagrande, L. K. Aagesen, J.-H. Ke, W. Jiang, J. D. Hales, A. Toptan, K. A.  
659 Gamble, X.-Y. Liu, S. R. Novascone, C. Matthews, D. S. Stafford, Summary of BISON  
660 milestones: NEAMS FY-20 report, Tech. rep., Idaho National Laboratory (2020).
- 661 [6] M. Samsel-Czekała, E. Talik, P. De, R. Troć, H. Misioruk, C. Sułkowski, Electronic  
662 structure and magnetic and transport properties of single-crystalline UN, Physical Review B 76 (2007) 144426. [doi:10.1103/PhysRevB.76.144426](https://doi.org/10.1103/PhysRevB.76.144426).
- 663 [7] R. A. Evarestov, A. I. Panin, A. V. Bandura, M. V. Losev, Electronic structure of  
664 crystalline uranium nitrides UN, U<sub>2</sub>N<sub>3</sub> and UN<sub>2</sub>: LCAO calculations with the basis  
665 set optimization, Journal of Physics: Conference Series 117 (2008). [doi:10.1088/1742-6596/117/1/012015](https://doi.org/10.1088/1742-6596/117/1/012015).
- 666 [8] D. Gryaznov, E. Heifets, E. Kotomin, The first-principles treatment of the electron-  
667 correlation and spin-orbital effects in uranium mononitride nuclear fuels, Physical Chemistry  
668 Chemical Physics 14 (2012) 4482–4490. [doi:10.1039/c2cp40297a](https://doi.org/10.1039/c2cp40297a).
- 669 [9] Z. G. Mei, M. Stan, B. Pichler, First-principles study of structural, elastic, electronic,  
670 vibrational and thermodynamic properties of UN, Journal of Nuclear Materials 440  
671 (2013) 63–69. [doi:10.1016/j.jnucmat.2013.04.058](https://doi.org/10.1016/j.jnucmat.2013.04.058).
- 672 [10] V. Kocevski, D. A. Rehn, M. W. D. Cooper, D. A. Andersson, First-principles investi-  
673 gation of uranium mononitride (UN): Effect of magnetic ordering, spin-orbit inter-  
674 actions and exchange correlation functional, Journal of Nuclear Materials 559 (2022).  
675 [doi:10.1016/j.jnucmat.2021.153401](https://doi.org/10.1016/j.jnucmat.2021.153401).
- 676 [11] E. A. Kotomin, R. W. Grimes, Y. Mastrikov, N. J. Ashley, Atomic scale DFT simulations  
677 of point defects in uranium nitride, Journal of Physics Condensed Matter 19 (2007).  
678 [doi:10.1088/0953-8984/19/10/106208](https://doi.org/10.1088/0953-8984/19/10/106208).
- 679 [12] E. A. Kotomin, Y. A. Mastrikov, S. N. Rashkeev, P. V. Uffelen, Implementing first-  
680 principles calculations of defect migration in a fuel performance code for UN simulations,  
681 Journal of Nuclear Materials 393 (2009) 292–299. [doi:10.1016/j.jnucmat.2009.06.016](https://doi.org/10.1016/j.jnucmat.2009.06.016).
- 682

- 686 [13] D. Bocharov, D. Gryaznov, Y. F. Zhukovskii, E. A. Kotomin, DFT calculations of point  
687 defects on UN(001) surface, *Surface Science* 605 (2011) 396–400. [doi:10.1016/j.susc.2010.11.007](https://doi.org/10.1016/j.susc.2010.11.007).
- 689 [14] J. H. Lan, Z. C. Zhao, Q. Wu, Y. L. Zhao, Z. F. Chai, W. Q. Shi, First-principles  
690 DFT+*U* modeling of defect behaviors in anti-ferromagnetic uranium mononitride, *Journal*  
691 of Applied Physics 114 (2013). [doi:10.1063/1.4846217](https://doi.org/10.1063/1.4846217).
- 692 [15] E. A. Kotomin, Y. A. Mastrikov, First principles modeling of oxygen impurities in  
693 UN nuclear fuels, *Journal of Nuclear Materials* 377 (2008) 492–495. [doi:10.1016/j.jnucmat.2008.04.015](https://doi.org/10.1016/j.jnucmat.2008.04.015).
- 695 [16] M. Klipfel, P. V. Uffelen, Ab initio modelling of volatile fission products in ura-  
696 nium mononitride, *Journal of Nuclear Materials* 422 (2012) 137–142. [doi:10.1016/j.jnucmat.2011.12.018](https://doi.org/10.1016/j.jnucmat.2011.12.018).
- 698 [17] A. Claisse, M. Klipfel, N. Lindbom, M. Freyss, P. Olsson, GGA+*U* study of uranium  
699 mononitride: A comparison of the U-ramping and occupation matrix schemes and incor-  
700 poration energies of fission products, *Journal of Nuclear Materials* 478 (2016) 119–124.  
701 [doi:10.1016/j.jnucmat.2016.06.007](https://doi.org/10.1016/j.jnucmat.2016.06.007).
- 702 [18] Y. J. Zhang, J. H. Lan, C. Z. Wang, Q. Y. Wu, T. Bo, Z. F. Chai, W. Q. Shi, Theoretical  
703 investigation on incorporation and diffusion properties of Xe in uranium mononitride,  
704 *Journal of Physical Chemistry C* 119 (2015) 5783–5789. [doi:10.1021/jp510219a](https://doi.org/10.1021/jp510219a).
- 705 [19] L. Yang, N. Kaltsoyannis, Incorporation of Kr and Xe in uranium mononitride: A  
706 density functional theory study, *Journal of Physical Chemistry C* 125 (2021) 26999–  
707 27008. [doi:10.1021/acs.jpcc.1c08523](https://doi.org/10.1021/acs.jpcc.1c08523).
- 708 [20] K. Kurosaki, K. Yano, K. Yamada, M. Uno, S. Yamanaka, A molecular dynamics study  
709 of the heat capacity of uranium mononitride, *Journal of Alloys and Compounds* 297  
710 (2000) 1–4.
- 711 [21] K. Kurosaki, K. Yano, K. Yamada, M. Uno, S. Yamanaka, A molecular dynamics study  
712 of the thermal conductivity of uranium mononitride, *Journal of Alloys and Compounds*  
713 311 (2000) 305–310.
- 714 [22] P. H. Chen, X. L. Wang, X. C. Lai, G. Li, B. Y. Ao, Y. Long, Ab initio interionic  
715 potentials for UN by multiple lattice inversion, *Journal of Nuclear Materials* 404 (2010)  
716 6–8. [doi:10.1016/j.jnucmat.2010.06.017](https://doi.org/10.1016/j.jnucmat.2010.06.017).
- 717 [23] Y. Mishin, *Interatomic Potentials for Metals*, Springer, 2005.
- 718 [24] A. Y. Kuksin, S. V. Starikov, D. E. Smirnova, V. I. Tseplyaev, The diffusion of point  
719 defects in uranium mononitride: Combination of DFT and atomistic simulation with  
720 novel potential, *Journal of Alloys and Compounds* 658 (2016) 385–394. [doi:10.1016/j.jallcom.2015.10.223](https://doi.org/10.1016/j.jallcom.2015.10.223).

- [25] V. I. Tseplyaev, S. V. Starikov, The atomistic simulation of pressure-induced phase transition in uranium mononitride, Journal of Nuclear Materials 480 (2016) 7–14. [doi:10.1016/j.jnucmat.2016.07.048](https://doi.org/10.1016/j.jnucmat.2016.07.048).
- [26] J. J. Li, S. T. Murphy, Diffusion in hypo-stoichiometric uranium mononitride, Progress in Nuclear Energy 142 (2021). [doi:10.1016/j.pnucene.2021.103995](https://doi.org/10.1016/j.pnucene.2021.103995).
- [27] V. Kocevski, M. W. Cooper, A. J. Claisse, D. A. Andersson, Development and application of a uranium mononitride (UN) potential: Thermomechanical properties and Xe diffusion, Journal of Nuclear Materials 562 (2022). [doi:10.1016/j.jnucmat.2022.153553](https://doi.org/10.1016/j.jnucmat.2022.153553).
- [28] A. P. Thompson, H. M. Aktulga, R. Berger, D. S. Bolintineanu, W. M. Brown, P. S. Crozier, P. J. in 't Veld, A. Kohlmeyer, S. G. Moore, T. D. Nguyen, R. Shan, M. J. Stevens, J. Tranchida, C. Trott, S. J. Plimpton, Lammps - a flexible simulation tool for particle-based materials modeling at the atomic, meso, and continuum scales, Computer Physics Communications 271 (2022). [doi:10.1016/j.cpc.2021.108171](https://doi.org/10.1016/j.cpc.2021.108171).
- [29] A. Togo, I. Tanaka, First principles phonon calculations in materials science, Scripta Materialia 108 (2015) 1–5. [doi:10.1016/j.scriptamat.2015.07.021](https://doi.org/10.1016/j.scriptamat.2015.07.021).
- [30] A. Carreras, A. Togo, I. Tanaka, DynaPhoPy: A code for extracting phonon quasi-particles from molecular dynamics simulations, Computer Physics Communications 221 (2017) 221–234. [doi:10.17632/v493dkxk8r.1](https://doi.org/10.17632/v493dkxk8r.1).
- [31] G. W. Silva, C. B. Yeamans, A. P. Sattelberger, T. Hartmann, G. S. Cerefice, K. R. Czerwinski, Reaction sequence and kinetics of uranium nitride decomposition, Inorganic Chemistry 48 (2009). [doi:10.1021/ic901165j](https://doi.org/10.1021/ic901165j).
- [32] S. L. Hayes, J. K. Thomas, K. L. Peddicord, Material property correlations for uranium mononitride I. physical properties, Journal of Nuclear Materials 171 (1990) 262–270.
- [33] S. L. Hayes, J. K. Thomas, K. L. Peddicord, Material property correlations for uranium mononitride IV. thermodynamic properties, Journal of Nuclear Materials 171 (1990) 300–318.
- [34] H. Tagawa, N. Masaki, X-ray and density studies of nonstoichiometric uranium sesquinitride, Journal of Inorganic and Nuclear Chemistry 36 (1974). [doi:10.1016/0022-1902\(74\)80220-4](https://doi.org/10.1016/0022-1902(74)80220-4).
- [35] C. E. Price, I. H. Warren, Some observations on uranium-nitrogen compounds, Inorganic Chemistry 4 (1965). [doi:10.1021/ic50023a028](https://doi.org/10.1021/ic50023a028).
- [36] N. Masaki, H. Tagawa, The structure of  $\{\beta\text{-U}_2\text{N}_3\}$ , Journal of Nuclear Materials 58 (1975). [doi:10.1016/0022-3115\(75\)90114-2](https://doi.org/10.1016/0022-3115(75)90114-2).
- [37] D. A. Weber, C. Schwickert, A. Senyshyn, M. Lerch, R. Pöttgen, Physical properties and lattice dynamics of bixbyite-type  $\text{V}_2\text{O}_3$ , Journal of Materials Research 32 (2017). [doi:10.1557/jmr.2017.144](https://doi.org/10.1557/jmr.2017.144).

- 759 [38] H. Okamoto, N-U (nitrogen-uranium), Journal of Phase Equilibria 18 (1997) 107.
- 760 [39] S. Alavi, D. L. Thompson, Simulations of melting of polyatomic solids and nanoparticles,  
761 Molecular Simulation 32 (2006). [doi:10.1080/08927020600823158](https://doi.org/10.1080/08927020600823158).
- 762 [40] Y. Zhang, E. J. Maginn, A comparison of methods for melting point calculation using  
763 molecular dynamics simulations, Journal of Chemical Physics 136 (2012). [doi:10.1063/1.3702587](https://doi.org/10.1063/1.3702587).
- 765 [41] F. Ercolessi, A molecular dynamics primer, Tech. rep., International Centre for Theoretical Physics (1997).
- 767 [42] S. J. Blundell, K. M. Blundell, Concepts in Thermal Physics, 2nd Edition, Oxford University Press, 2010.
- 769 [43] G. Clavier, N. Desbiens, E. Bourasseau, V. Lachet, N. Brusselle-Dupend, B. Rousseau,  
770 Computation of elastic constants of solids using molecular simulation: comparison of  
771 constant volume and constant pressure ensemble methods, Molecular Simulation 43  
772 (2017) 1413–1422. [doi:10.1080/08927022.2017.1313418](https://doi.org/10.1080/08927022.2017.1313418).
- 773 [44] M. A. Meyers, K. K. Chawla, Mechanical Behavior of Materials, 2nd Edition, Cambridge University Press, 2008.
- 775 [45] K. W. Böer, U. W. Pohl, Semiconductor Physics, Springer International Publishing AG,  
776 2018. [doi:<https://doi.org/10.1007/978-3-319-69150-3>](https://doi.org/10.1007/978-3-319-69150-3).
- 777 [46] O. L. Anderson, A simplified method for calculating the Debye temperature from elastic  
778 constants, Journal of Physics and Chemistry of Solids 24 (1963) 909–917.
- 779 [47] F. Mouhat, F.-X. Coudert, Necessary and sufficient elastic stability conditions in various  
780 crystal systems, Physical Review B - Condensed Matter and Materials Physics 90 (2014).  
781 [doi:10.1103/PhysRevB.90.224104](https://doi.org/10.1103/PhysRevB.90.224104).
- 782 [48] H. Siethoff, K. Ahlborn, The dependence of Debye temperature on elastic constants,  
783 Physica Status Solidi B 190 (1995) 179–191. [doi:10.1002/pssb.2221900126](https://doi.org/10.1002/pssb.2221900126).
- 784 [49] V. Kocevski, D. A. Rehn, A. J. Terricabras, A. van Veelen, M. W. Cooper, S. W.  
785 Paisner, S. C. Vogel, J. T. White, D. A. Andersson, Finite temperature properties of  
786 uranium mononitride, Journal of Nuclear Materials 576 (2023) 154241. [doi:10.1016/j.jnucmat.2023.154241](https://doi.org/10.1016/j.jnucmat.2023.154241).
- 788 [50] T. R. Pavlov, M. R. Wenman, L. Vlahovic, D. Robba, R. J. Konings, P. V. Uffelen,  
789 R. W. Grimes, Measurement and interpretation of the thermo-physical properties of  
790  $\text{UO}_2$  at high temperatures: The viral effect of oxygen defects, Acta Materialia 139  
791 (2017) 138–154. [doi:10.1016/j.actamat.2017.07.060](https://doi.org/10.1016/j.actamat.2017.07.060).
- 792 [51] M. S. Bryan, J. W. Pang, B. C. Larson, A. Chernatynskiy, D. L. Abernathy, K. Gofryk,  
793 M. E. Manley, Impact of anharmonicity on the vibrational entropy and specific heat of  
794  $\text{UO}_2$ , Physical Review Materials 3 (2019). [doi:10.1103/PhysRevMaterials.3.065405](https://doi.org/10.1103/PhysRevMaterials.3.065405).

- 795 [52] R. DeHoff, Thermodynamics in Materials Science, 2nd Edition, CRC Press, 2006.
- 796 [53] E. S. R. Gopal, Specific Heats at Low Temperatures, Springer US, 1966. [doi:10.1007/978-1-4684-9081-7\\_4](https://doi.org/10.1007/978-1-4684-9081-7_4).
- 798 [54] J. F. Counsell, R. M. Dell, J. F. Martin, Thermodynamic properties of uranium com-  
799 pounds part 2. low-temperature heat capacity and entropy of three uranium nitrides,  
800 Transactions of the Faraday Society 60 (1964) 1736–1747.
- 801 [55] J. O. Scarbrough, H. L. Davis, W. Fulkerson, J. O. Betterton, Specific heat of uranium  
802 mononitride from 1.3 to 4.6 K, Physical Review 176 (1968) 666–671.
- 803 [56] B. Szpunar, J. I. Ranasinghe, J. A. Szpunar, Electronic transport of uranium mononi-  
804 tride, Journal of Modern Physics 12 (2021). [doi:10.4236/jmp.2021.1210084](https://doi.org/10.4236/jmp.2021.1210084).
- 805 [57] F. Giustino, Materials Modelling using Density Functional Theory: Properties and  
806 Predictions, 1st Edition, Oxford University Press, 2014.
- 807 [58] E. Torres, I. CheikNjifon, T. P. Kaloni, J. Pencer, A comparative analysis of the phonon  
808 properties in  $\text{UO}_2$  using the Boltzmann transport equation coupled with DFT+ $U$  and  
809 empirical potentials, Computational Materials Science 177 (5 2020). [doi:10.1016/j.commatsci.2020.109594](https://doi.org/10.1016/j.commatsci.2020.109594).
- 810 [59] L. T. Kong, Phonon dispersion measured directly from molecular dynamics simulations,  
811 Computer Physics Communications 182 (2011). [doi:10.1016/j.cpc.2011.04.019](https://doi.org/10.1016/j.cpc.2011.04.019).
- 812 [60] A. Togo, L. Chaput, I. Tanaka, Distributions of phonon lifetimes in Brillouin zones,  
813 Physical Review B - Condensed Matter and Materials Physics 91 (2015). [doi:10.1103/PhysRevB.91.094306](https://doi.org/10.1103/PhysRevB.91.094306).
- 814 [61] Y. Mishin, D. Farkas, Atomistic simulation of point defects and diffusion in B2 NiAl  
815 part I. point defect energetics, Philosophical Magazine A 75 (1997) 169–185. [doi:10.1080/01418619708210289](https://doi.org/10.1080/01418619708210289).
- 816 [62] C. G. V. de Walle, J. Neugebauer, First-principles calculations for defects and impurities:  
817 Applications to III-nitrides, Journal of Applied Physics 95 (2004) 3851–3879. [doi:10.1063/1.1682673](https://doi.org/10.1063/1.1682673).
- 818 [63] S. Anand, J. P. Male, C. Wolverton, G. J. Snyder, Visualizing defect energetics, Mate-  
819 rials Horizons 8 (2021) 1966–1975. [doi:10.1039/d1mh00397f](https://doi.org/10.1039/d1mh00397f).
- 820 [64] B. Dorado, M. Freyss, G. Martin, GGA+ $U$  study of the incorporation of iodine in  
821 uranium dioxide, The European Physical Journal B 69 (2009) 203–209. [doi:10.1140/epjb/e2009-00145-0](https://doi.org/10.1140/epjb/e2009-00145-0).
- 822 [65] C. Freysoldt, B. Grabowski, T. Hickel, J. Neugebauer, G. Kresse, A. Janotti, C. G. V.  
823 de Walle, First-principles calculations for point defects in solids, Reviews of Modern  
824 Physics 86 (2014) 253–305. [doi:10.1103/RevModPhys.86.253](https://doi.org/10.1103/RevModPhys.86.253).

- 830 [66] M. Hagen, M. W. Finnis, Determination of the atomistic structure of the  $\Sigma 3$  (111) twin  
831 boundary in NiAl, Materials Science Forum 207-209 (1996) 245–248. [doi:10.4028/www.scientific.net/msf.207-209.245](https://doi.org/10.4028/www.scientific.net/msf.207-209.245).
- 833 [67] C. Woodward, S. Kajihara, L. H. Yang, Site preferences and formation energies of  
834 substitutional Si, Nb, Mo, Ta, and W solid solutions in  $L1_0$  Ti-Al, Physical Review B  
835 57 (1998).
- 836 [68] G. Y. Huang, G. Pastore, B. D. Wirth, First-principles study of intrinsic point defects  
837 and Xe impurities in uranium monocarbide, Journal of Applied Physics 128 (2020).  
838 [doi:10.1063/5.0021951](https://doi.org/10.1063/5.0021951).
- 839 [69] J. B. Wachtman, W. E. Tefft, D. G. Lam, C. S. Apstein, Exponential temperature  
840 dependence of Young's modulus for several oxides, Physical Review 122 (1961) 1754–  
841 1759.
- 842 [70] M. D. Salleh, J. E. Macdonald, G. A. Saunders, P. de V Du Plessis, Hydrostatic pres-  
843 sure dependences of elastic constants and vibrational anharmonicity of uranium nitride,  
844 Journal of Materials Science 21 (1986) 2577–2580.
- 845 [71] S. L. Hayes, J. K. Thomas, K. L. Peddicord, Material property correlations for uranium  
846 mononitride II. mechanical properties, Journal of Nuclear Materials 171 (1990) 271–288.
- 847 [72] A. Padel, C. de Novion, Constantes élastiques des carbures, nitrures et oxydes d'uranium  
848 et de plutonium, Journal of Nuclear Materials 33 (1969) 40–51.
- 849 [73] D. Frazer, B. Maiorov, U. Carvajal-Nuñez, J. Evans, E. Kardoulaki, J. Dunwoody, T. A.  
850 Saleh, J. T. White, High temperature mechanical properties of fluorite crystal structured  
851 materials ( $CeO_2$ ,  $ThO_2$ , and  $UO_2$ ) and advanced accident tolerant fuels ( $U_3Si_2$ , UN, and  
852  $UB_2$ ), Journal of Nuclear Materials 554 (2021). [doi:10.1016/j.jnucmat.2021.153035](https://doi.org/10.1016/j.jnucmat.2021.153035).
- 853 [74] C. Zener, Contributions to the theory of beta-phase alloys, Physical Review 71 (1947).  
854 [doi:10.1103/PhysRev.71.846](https://doi.org/10.1103/PhysRev.71.846).
- 855 [75] H. L. Whaley, W. Fulkerson, R. A. Potter, Elastic moduli and Debye temperature of  
856 polycrystalline uranium nitride by ultrasonic velocity measurements, Journal of Nuclear  
857 Materials 31 (1969). [doi:10.1016/0022-3115\(69\)90234-7](https://doi.org/10.1016/0022-3115(69)90234-7).
- 858 [76] E. F. Westrum, C. M. Barber, Uranium mononitride: Heat capacity and thermodynamic  
859 properties from 5 to 350 K, The Journal of Chemical Physics 45 (1966) 635–639.
- 860 [77] V. G. Baranov, Y. N. Devyatko, A. V. Tenishev, A. V. Khlunov, O. V. Khomyakov, A  
861 physical model for evaluating uranium nitride specific heat, Journal of Nuclear Materials  
862 434 (2013). [doi:10.1016/j.jnucmat.2012.10.047](https://doi.org/10.1016/j.jnucmat.2012.10.047).
- 863 [78] D. P. Sellan, E. S. Landry, J. E. Turney, A. J. McGaughey, C. H. Amon, Size effects in  
864 molecular dynamics thermal conductivity predictions, Physical Review B - Condensed  
865 Matter and Materials Physics 81 (2010). [doi:10.1103/PhysRevB.81.214305](https://doi.org/10.1103/PhysRevB.81.214305).

- 866 [79] C. Galvin, N. Kuganathana, N. Barronc, R. W. Grimes, Predicted thermophysical prop-  
867 erties of UN, PuN and (U, Pu)N (2023).
- 868 [80] J. A. Jackman, T. M. Holden, J. I. Buyers, P. de V. DuPlessis, O. Vogt, J. Genossar,  
869 Systematic study of the lattice dynamics of the uranium rocksalt-structure compounds,  
870 Physical Review B 33 (1986) 7144–7153.
- 871 [81] A. A. Aczel, G. E. Granroth, G. J. MacDougall, W. J. Buyers, D. L. Abernathy, G. D.  
872 Samolyuk, G. M. Stocks, S. E. Nagler, Quantum oscillations of nitrogen atoms in ura-  
873 nium nitride, Nature Communications 3 (2012). [doi:10.1038/ncomms2117](https://doi.org/10.1038/ncomms2117).
- 874 [82] X. W. Zhou, S. Aubry, R. E. Jones, A. Greenstein, P. K. Schelling, Towards more  
875 accurate molecular dynamics calculation of thermal conductivity: Case study of {GaN}  
876 bulk crystals, Physical Review B - Condensed Matter and Materials Physics 79 (2009).  
877 [doi:10.1103/PhysRevB.79.115201](https://doi.org/10.1103/PhysRevB.79.115201).
- 878 [83] N. W. Ashcroft, N. D. Mermin, Solid State Physics, 1st Edition, Cengage Learning,  
879 1976.
- 880 [84] X. Li, P. F. Liu, E. Zhao, Z. Zhang, T. Guidi, M. D. Le, M. Avdeev, K. Ikeda, T. Otomo,  
881 M. Kofu, K. Nakajima, J. Chen, L. He, Y. Ren, X. L. Wang, B. T. Wang, Z. Ren,  
882 H. Zhao, F. Wang, Ultralow thermal conductivity from transverse acoustic phonon  
883 suppression in distorted crystalline  $\alpha$ -MgAgSb, Nature Communications 11 (2020). [doi:  
884 10.1038/s41467-020-14772-5](https://doi.org/10.1038/s41467-020-14772-5).
- 885 [85] Z. Tian, K. Esfarjani, J. Shiomi, A. S. Henry, G. Chen, On the importance of optical  
886 phonons to thermal conductivity in nanostructures, Applied Physics Letters 99 (2011).  
887 [doi:10.1063/1.3615709](https://doi.org/10.1063/1.3615709).
- 888 [86] S. L. Hayes, J. K. Thomas, K. L. Peddicord, Material property correlations for uranium  
889 mononitride III. transport properties, Journal of Nuclear Materials 171 (1990) 289–299.
- 890 [87] F. A. Kröger, H. J. Vink, Relations between the concentrations of imperfections in  
891 crystalline solids, Solid State Physics - Advances in Research and Applications 3 (1956).  
892 [doi:10.1016/S0081-1947\(08\)60135-6](https://doi.org/10.1016/S0081-1947(08)60135-6).
- 893 [88] J. T. White, A. T. Nelson, J. T. Dunwoody, D. D. Byler, D. J. Safarik, K. J. McClellan,  
894 Thermophysical properties of U<sub>3</sub>Si<sub>2</sub> to 1773 K, Journal of Nuclear Materials 464 (2015).  
895 [doi:10.1016/j.jnucmat.2015.04.031](https://doi.org/10.1016/j.jnucmat.2015.04.031).
- 896 [89] Y. Lu, B. T. Wang, R. W. Li, H. L. Shi, P. Zhang, Structural, electronic, mechanical, and  
897 thermodynamic properties of UN<sub>2</sub>: Systematic density functional calculations, Journal  
898 of Nuclear Materials 410 (2011) 46–51. [doi:10.1016/j.jnucmat.2010.12.308](https://doi.org/10.1016/j.jnucmat.2010.12.308).
- 899 [90] J. Rösler, H. Harders, M. Bäker, Mechanical Behaviour of Engineering Materials,  
900 Springer, 2007.

901 [91] H. E. Rosinger, D. O. Northwood, The elastic properties of zirconium alloy fuel cladding  
902 and pressure tubing materials, Journal of Nuclear Materials 79 (1979). [doi:10.1016/0022-3115\(79\)90444-6](https://doi.org/10.1016/0022-3115(79)90444-6).

904 [92] C. Kittel, Introduction to Solid State Physics, 8th Edition, John Wiley & Sons, Inc,  
905 2005.